

Three Visual Methods: Envisioning Tensors © Creating Eigenvalue-Eigenvector Glyphs

Envisioning second-, fourth-, and sixth-order tensors, and tensor equation invariance.

- [Envisioning Second-Order Stress Tensors, \$\sigma_{ij}\$](#)
 - [Principal Stress State](#)
 - [Point Stress Tensor Glyphs: Quadric, Haber, Reynolds, HWY, PNS](#)
 - [Quadric Surface Glyphs: Equilibrium Defines Shape](#)
 - [Haber Glyphs: Elliptical Disks and Rods \("keep it simple"\)](#)
 - [Reynolds Stress Tensor Glyphs: Normal Stresses Define Shape](#)
 - [HWY Glyphs: Shear Stresses Define Shape](#)
 - [PNS Glyphs: Principal Normal Stresses Define Ellipsoidal Shape](#)
 - [Second-Order Stress Tensor Gradients](#)
 - [Continuous Stress Tensor Glyphs in One Dimension: Tensor Tubes](#)
 - [Point Stress Tensor Gradients in Three Dimensions: Equilibrium](#)
 - [Envisioning Fourth-Order Stiffness Tensors, \$C_{ijkl}\$](#)
 - [Envisioning Sixth-Order Stress Induced Anisotropy Tensors, \$D_{ijklmn}\$](#)
-

In physics, engineering, chemistry, and the other physical sciences we frequently encounter the eigenvalue problem when we mathematically model physical systems. Structural design engineers encounter the eigenvalue problem when determining the principle stress state in deformable bodies. In fluid dynamics we encounter the rate of deformation tensor for fluid particles moving through Eulerian space. In wave propagation we encounter anisotropic wave velocity surfaces and particle vibration directions. Although these are all different physical systems, they have one thing in common: the mathematical model of the physical system typically results in an eigenvalue problem whose eigenvalues and eigenvectors are representative of physical properties. Often these eigenvalues-eigenvectors are embedded in much larger more complex systems where it would be of value if we could isolate the eigenvalue-eigenvectors by a glyph representation yet observe the glyph's relationship to it's surrounding functional space. Superimposed on these eigenvalue-eigenvector glyphs we can represent additional properties that show the relationship of the glyph to its surroundings. For example, a local component of the commoving derivative of a fluid particle could be represented by color mapped onto the strain rate glyph. Below we construct an illustrative example where we show how the principle stress state in a solid can be represented by an ellipsoid glyph whose shape represents the eigenvalues and whose orientation represents the direction of a principal stress state. The reader is encouraged to experiment with adding other properties to their glyphs. Rarely do eigenvalues-eigenvectors properties occur as isolated events in the physical systems that we study and model. Such a systematic rational approach leads to insight. If this technique is applicable to other systems in general, then this technique becomes a methodology: a visual methodology.

Envisioning Second-Order Stress Tensors, σ_{ij}

Principal Stress State

Second order tensors can be used to represent the state of stress and strain, in Lagrangian space or stress and strain rate in Eulerian space. Here a Lagrangian approach is used where the components of any second order stress tensor can be reduced to an eigenvalue problem and visualized as a quadric surface, Frederick and Chang [8]. The components of a stress tensor can be written in a more familiar matrix format where it is useful to show how each matrix term is a vector component acting on the differential element shown in Fig. 27.

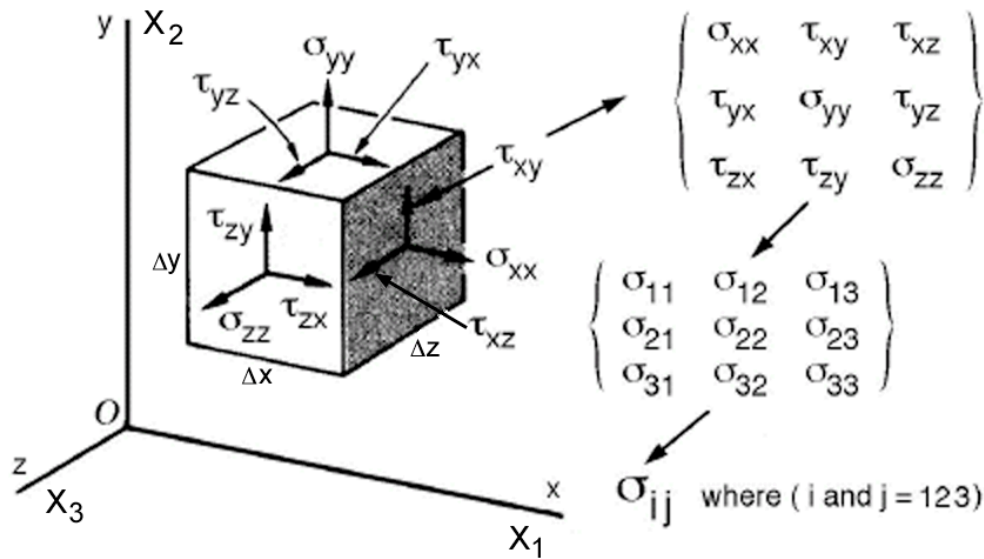


Figure 27. Stress tensor components shown on differential element.

When written in indicial notation, σ_{ij} , this second order tensor obeys the transformation law, Eqn. (10), where a_{ij} is the rotational transformation matrix. Not all matrices reduced to tensors. A quantity can only be called a tensor if its components obey the tensor transformation law.

$$\sigma'_{ij} = a_{ir} a_{js} \sigma_{rs} \tag{10}$$

When rotated the rectangular cartesian coordinates, X_i , transform as first order tensors.

$$X'_i = a_{ij} X_j \tag{11}$$

The term a_{ij} is the rotational transformation matrix defined in most tensor theory textbooks. It is important to note that this transformation matrix does not include translation as a fourth row and column, which is typically used in most computer graphic software APIs (Application Programming Interfaces). In the development that follows the relationship between this transformation matrix and Euler angle will be used to rotate stress tensor glyphs into principal stress states.

Here the second order stress tensor is transformed into an eigenvalue-eigenvector problem using tensor notation instead of matrices because of its notational brevity. For the reader who is more familiar with the matrix approach we leave this as an exercise where the reader can refer to any standard text on deformable bodies. Schaums outline on Continuum Mechanics, Mase [9], develops the principal stress eigenvalue problem using both matrices and tensors.

Stress can be represented both as a first order tensor, σ_i (vector), and as a second order tensor, σ_{ij} . These two types of stresses can be related by cutting the differential element in Fig. 27 and applying a stress vector on the cut plane (P_1, P_2, P_3) , Fig. 28. To maintain equilibrium the second order stress tensor components, shown on the opposite facing surfaces as dashed lines, must be equal to the direction cosine components of the first order stress tensor acting on the titled plane (P_1, P_2, P_3) . The orientation of the tilted plane is arbitrary and defined by the direction cosines of the unit normal vector, n_j . Imagine that as the plane (P_1, P_2, P_3) is tilted the magnitude and direction of σ_i changes to maintain equilibrium with the second order stress tensor components which are shown as dashed lines on the opposite facing surfaces. Note the components of the second order stress tensor do not change as the plane tilts. This equation should be called the equilibrium equation, however to honor the accomplishments of a famous mathematician, Augustin-Louis Cauchy (1789-1857), this relationship is called Cauchy's equation (12).

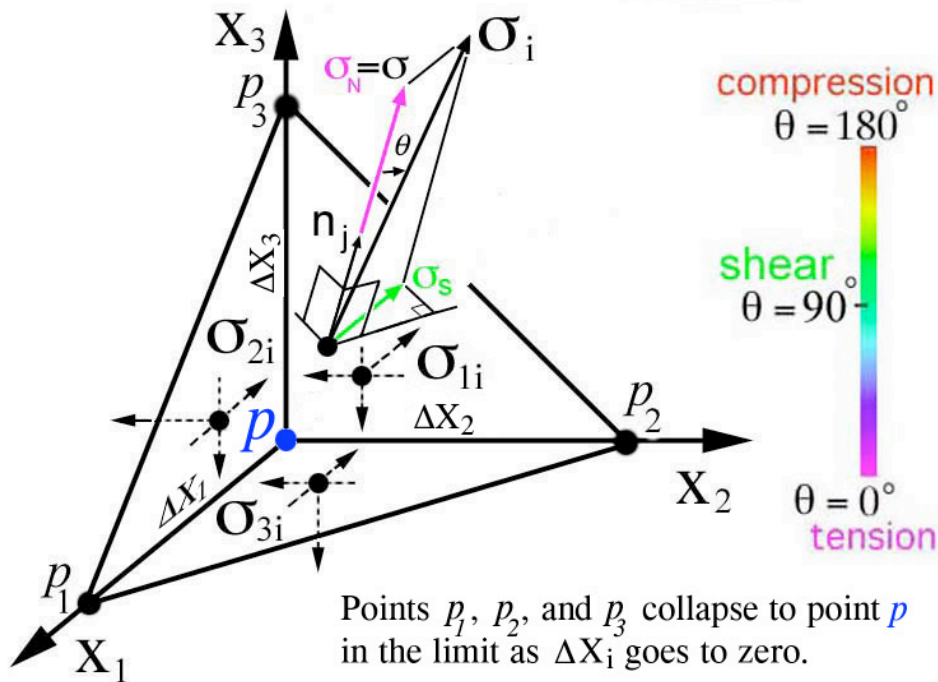


Figure 28. Stress, σ_i , vector acting on a titled plane (P_1, P_2, P_3) in equilibrium with the components of the second order stress tensor, σ_{ij} . Color legend used to indicate stress type (tension, shear, compression)

$$\sigma_i = \sigma_{ji} n_j \tag{12}$$

In general σ_i and n_j are oriented in different directions and the first order stress tensor, σ_i , can be resolved into normal and shear components, (σ_N, σ_S) . However the plane (P_1, P_2, P_3) can be oriented such that the first order stress tensor σ_i , and the unit vector, n_j , are parallel and the shear component goes to zero, $\sigma_S = 0$. This special direction defines principal stress, σ , when $\sigma_S = 0$. This principal stress can also be referred to as σ_N , however traditionally the symbol σ is used in the development of the eigen-value problem.

$$\sigma_i = \sigma n_i, \text{ where } \sigma = \sigma_N \quad (13)$$

This special case is referred to as a principal direction where the magnitude of this stress, σ , is called a principal stress, which is the scalar component of σ_i projected onto the unit vector n_i . The color legend will prove useful when envisioning stress type as a color gradient projected onto various stress glyph surfaces. Development of the eigen-value problem continues using the principal stress, σ , without the use of color. Equating Eqn.s (12) and (13) and rearranging indices on n_i using the Kronecker delta, δ_{ij} , yields

$$\sigma_i = \sigma_{ji} n_j = \sigma \delta_{ij} n_j \quad (14)$$

$$(\sigma_{ji} - \sigma \delta_{ij}) n_j = 0 \quad (15)$$

The Kronecker delta, δ_{ij} , is equivalent to the identity matrix. Together with the orthogonality conditions there are four equations with four unknowns. Equation (15) becomes an eigenvalue problem which can be rewritten here in a more familiar matrix notation,

$$\begin{bmatrix} \sigma_{11} - \sigma & \sigma_{12} & \sigma_{13} \\ \sigma_{21} & \sigma_{22} - \sigma & \sigma_{23} \\ \sigma_{31} & \sigma_{32} & \sigma_{33} - \sigma \end{bmatrix} \begin{Bmatrix} n_1 \\ n_2 \\ n_3 \end{Bmatrix} = 0 \quad (16)$$

where the stress scalar terms, σ , along the diagonal are the three eigenvalues (principal stresses: $\sigma_a, \sigma_b, \sigma_c$) and the column vector are the eigenvectors (direction cosines: "orientations" of the principal stress state). When the differential element shown in Fig. 27 is rotated into the principal stress state the normal stresses, σ_{xx} , σ_{yy} , and σ_{zz} become maximums and minimums ($\sigma_a, \sigma_b, \sigma_c$) and the shear stresses go to zero as shown on the cube to the right in Fig. 29.

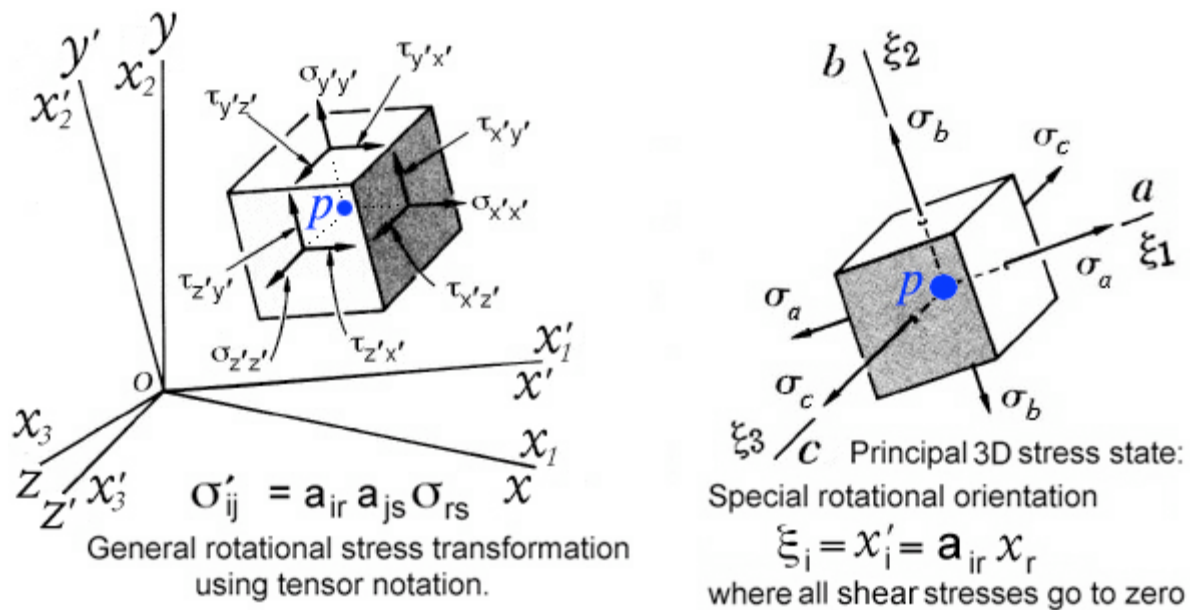


Figure 29. Rotation of differential element into the principal stress state.

This eigen-value problem is very common and there are numerous text books on numerical methods that solve for the eigen-values and eigen-vectors. Here the numerical solution is developed first followed by development of customized stress tensor "glyphs" that will hopefully provide insight from a scientific point of view. The development of the numerical solution follows.

Here a computer program is developed to solve for eigen-values and eigen-vectors using a standard Jacobi method. The complete program ([eigen.f](#)), sample data set ([sij.data](#)), and corresponding results ([eigen-calc-details.out](#), [eigen-stress.out](#), [eigen-vectors.out](#)) can be downloaded and used to reproduce results shown here. Below we discuss the solution using code fragments.

The solutions assumes symmetric stress tensors therefore only six components are read in the order shown in the code fragment below followed by the stress location at coordinates x, y, and z. Here the notation for stress, $a(i,j)$, is unfortunately the same notation used for the rotational transformation matrix, a_{ij} . However this notation is only used in the code to be consistent with the notation used by subroutine jacobi.

```

c
c read and establish starting matrix a
  do 2 i=1,3
  do 2 j=1,3
    evect(i,j)=0.0
    eval(i)=0.0
  2 a(i,j)=0.0
c
c all matrices are second order stress tensors, n=3
  n=3
  read(5,101)a(1,1),a(2,2),a(3,3),a(1,2),a(1,3),a(2,3),
*x(im),y(im),z(im)
  a(2,1)=a(1,2)
  a(3,1)=a(1,3)
  a(3,2)=a(2,3)
  write(6,200) n,itmax,eps1,eps2,eps3
  do 3 i=1,n
  3 write(6,201) (a(i,j),j=1,n)
c

```

```

c compute eigenvalues and eigenvectors
call jacobi(n,a,eval,evect,itmax,eps1,eps2,eps3)

```

Given the nine components, $n=3$ (3 rows and columns), of the stress tensor, $a(i,j)$, subroutine jacobi returns a total of three eigen-values and a corresponding set of three eigen-vectors. For each i -th eigen-value, $eval(i)$, there is a corresponding eigen-vector, $evect(i,j)$, with three components, $j=1,2,3$.

These eigen-vector components correspond to the direction cosines, ξ_j , in Eqn (16) which defines the orientation of the plane (P_1, P_2, P_3) in Fig. 28, when $\sigma_S = 0$. Since there are three eigen-values there is a set of three eigen-vectors, $evect(i,j)$, that define the directions of the three principal planes shown in Fig. 29. Together this collection of direction cosines is equivalent to the rotational transformation matrix, a_{ij} , used in Eqn.s (10) and (11). From this transformation matrix, a_{ij} , Euler angles are calculated. Euler angles are the preferred method of rotating three-dimensional objects in many graphic programs. Below we develop a general method for extracting Euler angles from a transformation matrix, a_{ij} .

Given: a_{ij} , **Find:** Euler angles $(\theta_x, \theta_y, \theta_z)$. This is accomplished by creating a transformation matrix, a_{ij} , from a sequence of three simple rotations in Fig. 30. Because the rotation matrix, a_{ij} , is constructed from Euler angle rotations, these angles can be extracted from this matrix using simple algebra. Here we use the same procedure and notation outlined by Bourke [10]. The coordinate system shown in Fig. 30 is typically used in flight simulators with the origin located at the aircraft centroid, with the y-axis pointing forward, the x-axis off the right wing and the z-axis pointing up. Rotation sequence is as follows: (1) "roll" positive to the right, (2) "pitch" positive up, and (3) "yaw" positive to the left. Note: order matters, (1) \rightarrow (2) \rightarrow (3) is not equal to (2) \rightarrow (1) \rightarrow (3).

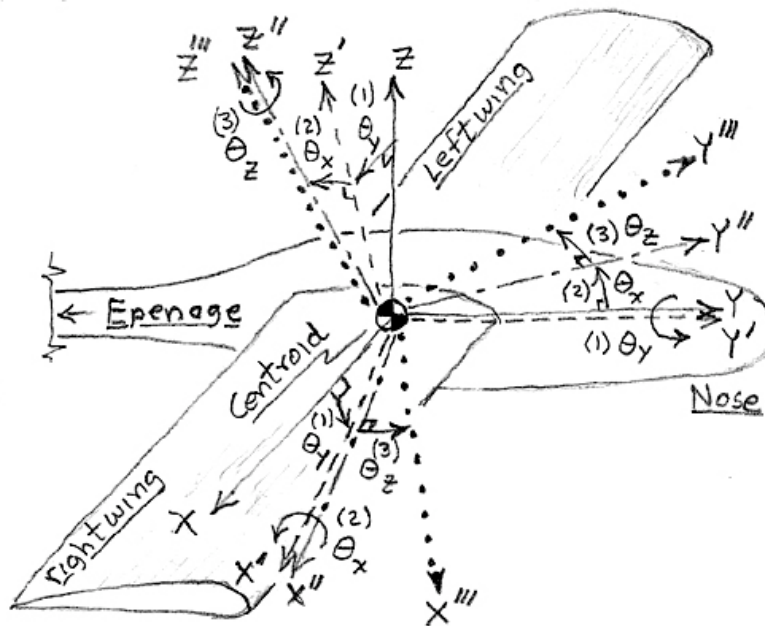


Figure 30. Standard flight simulator coordinates and Euler angle rotations: (1) roll, (2) pitch, (3) yaw.

Rotation sequence as experienced by a pilot sitting in the airplane cockpit, Fig. 30: (1) roll right, $+\theta_y$, Eqn. (17), (2) pitch up, $+\theta_x$, Eqn. (18), (3) yaw left, "heading", $+\theta_z$, Eqn. (19). In reverse order this orientation is known as heading-pitch-roll (HPR).

$$\begin{Bmatrix} X' \\ Y' \\ Z' \end{Bmatrix} = \begin{bmatrix} \cos(\theta_y) & 0 & -\sin(\theta_y) \\ 0 & 1 & 0 \\ \sin(\theta_y) & 0 & \cos(\theta_y) \end{bmatrix} \begin{Bmatrix} X \\ Y \\ Z \end{Bmatrix} \quad (17), \quad \begin{Bmatrix} X'' \\ Y'' \\ Z'' \end{Bmatrix} = \begin{bmatrix} 1 & 0 & 0 \\ 0 & \cos(\theta_x) & \sin(\theta_x) \\ 0 & -\sin(\theta_x) & \cos(\theta_x) \end{bmatrix} \begin{Bmatrix} X' \\ Y' \\ Z' \end{Bmatrix} \quad (18),$$

$$\begin{Bmatrix} X''' \\ Y''' \\ Z''' \end{Bmatrix} = \begin{bmatrix} \cos(\theta_z) & \sin(\theta_z) & 0 \\ -\sin(\theta_z) & \cos(\theta_z) & 0 \\ 0 & 0 & 1 \end{bmatrix} \begin{Bmatrix} X'' \\ Y'' \\ Z'' \end{Bmatrix} \quad (19).$$

For brevity the following notation is used, for cosines: $ctx = \cos(\theta_x)$, $cty = \cos(\theta_y)$, $ctz = \cos(\theta_z)$, and for sines: $stx = \sin(\theta_x)$, $sty = \sin(\theta_y)$, $stz = \sin(\theta_z)$. Combine roll followed by pitch.

$$\begin{bmatrix} cty & 0 & -sty \\ (stx)(sty) & ctx & (stx)(cty) \\ (ctx)(sty) & -stx & (ctx)(cty) \end{bmatrix} = \begin{bmatrix} 1 & 0 & 0 \\ 0 & ctx & stx \\ 0 & -stx & ctx \end{bmatrix} \begin{bmatrix} cty & 0 & -sty \\ 0 & 1 & 0 \\ sty & 0 & cty \end{bmatrix} \quad (20),$$

$$\begin{Bmatrix} X'' \\ Y'' \\ Z'' \end{Bmatrix} = \begin{bmatrix} cty & 0 & -sty \\ (stx)(sty) & ctx & (stx)(cty) \\ (ctx)(sty) & -stx & (ctx)(cty) \end{bmatrix} \begin{Bmatrix} X \\ Y \\ Z \end{Bmatrix} \quad (21)$$

Combine the roll and pitch transformation (20) above with the yaw transformation (19).

$$\begin{bmatrix} (ctx)(cty) + (stz)(stx)(sty) & (stz)(ctx) & -(ctx)(sty) + (stz)(stx)(cty) \\ -(stz)(cty) + (ctx)(stx)(sty) & (ctx)(ctx) & (stz)(stz) + (ctx)(stx)(cty) \\ (ctx)(sty) & -stx & (ctx)(cty) \end{bmatrix} = \begin{bmatrix} ctz & stz & 0 \\ -stz & ctx & 0 \\ 0 & 0 & 1 \end{bmatrix} \begin{bmatrix} cty & 0 & -stz \\ (stx)(sty) & ctx & (stx)(cty) \\ (ctx)(sty) & -stx & (ctx)(cty) \end{bmatrix} \quad (22)$$

Combining all three transformations (1) -> (2) -> (3) yields the final transformation $X_i = a_{ij} X_j$, where $a_{11} = (ctx)(cty) + (stz)(stx)(sty)$, $a_{12} = (stz)(ctx)$, $a_{13} = -(ctx)(sty) + (stz)(stx)(cty)$, etc..

$$\begin{Bmatrix} X''' \\ Y''' \\ Z''' \end{Bmatrix} = \begin{bmatrix} (ctx)(cty) + (stz)(stx)(sty) & (stz)(ctx) & -(ctx)(sty) + (stz)(stx)(cty) \\ -(stz)(cty) + (ctx)(stx)(sty) & (ctx)(ctx) & (stz)(stz) + (ctx)(stx)(cty) \\ (ctx)(sty) & -stx & (ctx)(cty) \end{bmatrix} \begin{Bmatrix} X \\ Y \\ Z \end{Bmatrix} \quad (23)$$

Recall notation $-stx = -\sin(\theta_x) = +a_{32}$ and collecting terms a_{31}/a_{33} and a_{12}/a_{22} , reduces terms to $a_{31}/a_{33} = [\cos(\theta_x) \sin(\theta_y)] / [\cos(\theta_x) \cos(\theta_y)] = \tan(\theta_y)$, and $a_{12}/a_{22} = \tan(\theta_z)$, and yields Euler angles as functions of components of the transformation matrix, a_{ij} .

$$\begin{aligned} \theta_x &= \sin^{-1}(-a_{32}) \\ \theta_y &= \tan^{-1}(a_{31} / a_{33}) \\ \theta_z &= \tan^{-1}(a_{12} / a_{22}) \end{aligned} \quad (24)$$

Recall the components of the transformation matrix, a_{ij} are equivalent to the set of three eigen-vectors and can be used to calculate the Euler angles.

```

c
c calculate Euler angles (degrees) from eigenvector (transformation matrix)
c
    aa=evect(3,1)/evect(3,3)
    eulerangy=180.0*atan(aa)/pi
    aa=-evect(3,2)
    eulerangx=180.0*asin(aa)/pi
    aa=evect(1,2)/evect(2,2)
    eulerangz=180.0*atan(aa)/pi
c
c calculate Euler angles (radians)
c
    eulernangyrad=eulerangy*pi/180.0
    eulernangxrad=eulerangx*pi/180.0
    eulernangzrad=eulerangz*pi/180.0

```

It is important to recall that the Eqn. (23) requires the rotation order, θ_y , θ_x , θ_z be used when implementing the rotation defined by the eigen-vectors orientation of the principal stress state.

This completes the mathematical solution of the eigen-value solution of Eqn. (16). Using these eigen-value and eigen-vector solutions, second order stress tensor "glyphs" are developed next that emphasize different physical properties of interest for the analysis of large data sets (insight) and for presentation of results.

The eigen-value problem defined in Eqn. (16) appears frequently in the applied sciences. Depending on the application the coefficient matrix consists of different physical quantities. Although the mathematics provides a common method for solving for the eigen-values and eigen-vectors, it is important to maintain the physical context when creating a graphical representation (glyph) of a physical property. It is often this context that leads to insight from the scientists who are visualizing their complex data sets for the first time. This is why the ESM4714 class is named "Scientific Visual Data Analysis" and just not "Visualization" or "Information Visualization". To be insightful from a scientific perspective the word scientific is used to qualify the type of data analysis. This also explains why the development here continues with a focus on the physical concepts of equilibrium and how the components of stress are visualized as normal and shear components that exist within the definition of a stress quadric surface, e.g. stress tensor glyphs. Several researchers [8,11,13,14] have demonstrated the usefulness of visualizing second order tensor glyphs. In all these studies glyphs revealed information that went beyond the initial physical understanding of the problem. Hence these studies demonstrated how glyphs provided insight that went beyond the traditional use of graphics, namely: graphics for presentation. In the final section these ideas are extended to higher order tensors. Through out the development of tensor glyphs the idea of invariance of tensor equations is used to envision important physical properties and relations between these physical properties as laws.

Point Stress Tensor Glyphs: Quadric, Haber, Reynolds, HWY, PNS

The development of the eigen-value problem required that all properties exist at points. For example in Fig. 28 points P_1 , P_2 , and P_3 collapse to point P in the limit as ΔX_i goes to zero. Therefore the equilibrium equation (12) exists at point P and the transformation of stress, Eqn. (10) also exists at a the same point in Fig. 29. Hence the development of all glyphs are envisioned as representing stress at their geomtric centroid, point P . Each glyph will be developed in the order they where published: Quadric, Haber, Reynolds, HWY, PNS.

Quadric Surface Glyphs: Equilibrium Defines Shape

The quadric surface was developed first by Frederick and Chang [8] as a tensor equation that exhibited two insightful properties. These properties were developed to envision, (1) eigen-values as shapes, (2) eigen-vectors as the 3D orientation of the principal stress state, and (3) the concept of equilibrium which was developed in Fig. 28 as a visual representation of the variation in the direction of first order stress tensor, σ_i , with respect to the unit vector, n_i to maintain a force balance with the components of the second order tensor, σ_{ij} . It is useful to review that, to avoid a trivial solution for principal stresses ($\sigma_a, \sigma_b, \sigma_c$), the determinant of the coefficient matrix in Eqn. (16) must be zero, which is written below in both tensor and expanded matrix notation,

$$| \sigma_{ij} - \sigma \delta_{ij} | = 0 \quad (25)$$

$$\begin{vmatrix} \sigma_{11} - \sigma & \sigma_{12} & \sigma_{13} \\ \sigma_{21} & \sigma_{22} - \sigma & \sigma_{23} \\ \sigma_{31} & \sigma_{32} & \sigma_{33} - \sigma \end{vmatrix} = 0 \quad (26)$$

Here the eigen-values can be determined by expanding the determinate into a polynomial cubic equation, which is a function of the second order stress components, σ_{ij} , and σ^3 . This is called the characteristic equation whose roots are numerically the same as the eigen-values solved for in Eqn. (16). These roots or eigen-values together with the principal directions can be visualized as a quadric surface, $F(\xi_i)$, which like the characteristic equation is also a scalar function of the components of the second order stress tensor, σ_{ij} .

$$F(\xi_i) = \sigma_{ij} \xi_i \xi_j = k^2 \quad (27)$$

This quadric surface is envisioned as an elliptical "glyph" in Fig. 31, whose major and minor axis lengths are functions of the eigen-values ($\sigma_a, \sigma_b, \sigma_c$) and orientation of these axes (ξ_1, ξ_2, ξ_3) are the eigen-vectors. Frederick and Chang [8] outline two additional properties that add insight to the relationship between stress as a first and second order tensor.

Property (i) Let Q be a point on the quadric surface, and let the distance $PQ = r$. Then the stress, σ_i , at P acting across the surface normal to PQ is inversely proportional to the radius vector, r, squared.

Property (ii) The stress vector at P, acting across the area that is normal to PQ, is parallel to the normal to the surface of the stress quadric at Q, see Fig. 31.

Note: both properties are related to the shape of the quadric surface which is defined by the components of the second order stress tensor, σ_{ij} . Proofs of these two properties are also insightful from an analytic point of view.

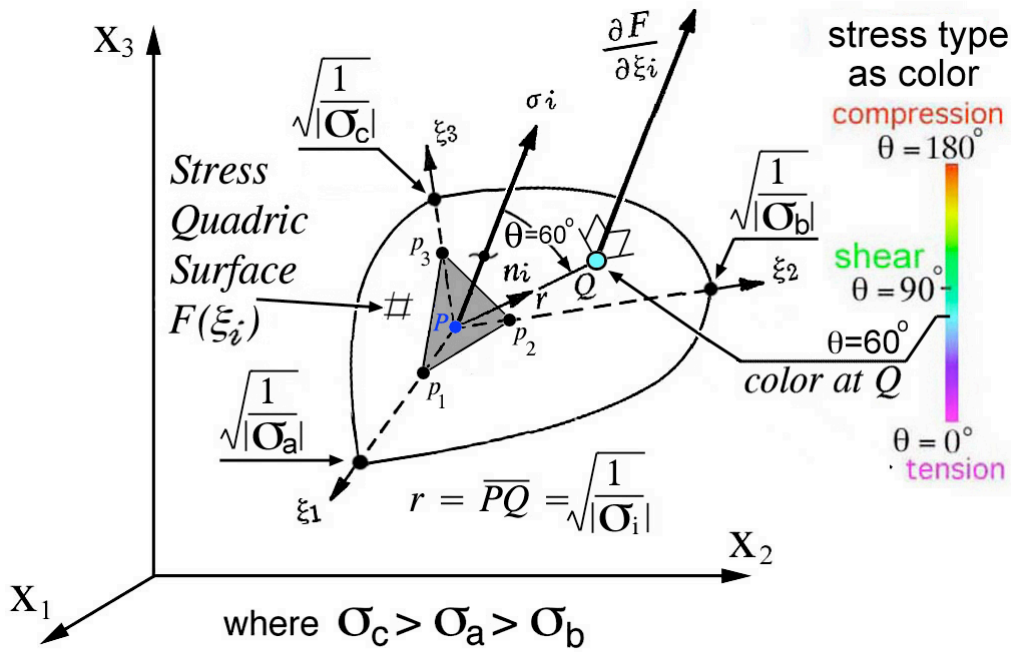


Figure 31. Stress tensor quadric surface "glyph" from Fredrick and Chang [8].

In summary the stress shown as a first order tensor, σ_i , is parallel to the gradient of scalar function, $F(\xi_i)$, which is perpendicular to the quadric surface. Since the shape of the quadric surface is a function of the second order stress tensor, σ_{ij} , the relationship between σ_i and σ_{ij} is envisioned as collection of all orientations of the plane (P_1, P_2, P_3) pointing in the direction of n_i . Since Cauchy's relationship, Eqn. (12), relates σ_i and σ_{ij} by the same unit vector, n_i , then the shape of the quadric surface (σ_{ij}) and the direction of lines (σ_i) perpendicular to same surface can be used to envision Cauchy's relationship in all possible directions. Since Cauchy's relationship is the essence of equilibrium and equilibrium is a law that exists in all possible directions, then the quadric surface with the vectors normal to the surface envisions equilibrium in all possible directions. **The quadric surface is equilibrium envisioned at a point.** Since Eqn. (27) is a tensor equation and all tensor equations are invariant to any arbitrary transformation, this invariance is envisioned in the same way that equilibrium is envisioned.

Again the idea of a gradient is an important concept used here to envision that the gradient of the quadric surface is pointing in the same direction as, σ_i . It is possible to draw a collection of short lines perpendicular to the quadric surface that shows all of these directions for all n_i , however the same color mapping developed in Fig. 28 can be used instead, which accomplishes the same result. Perhaps the color gradient would be easier to cognitively process than a "porcupine" glyph. An example of a principal stress state, $[\sigma_a, \sigma_b, \sigma_c] = [+1, +2, +3]$, is shown in Fig. 32 using color gradients to envision θ for all possible n_i and associated first and second order stress tensors.

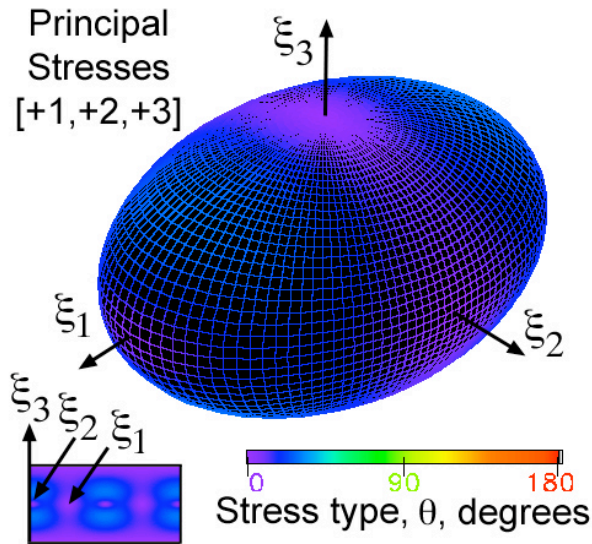


Figure 32. Stress quadric surface ellipsoid of [+1,+2,+3]

Creating the necessary topology, vertices and polygons, and color mapped onto these topologies is essentially the same for all of the tensor glyphs developed here. Here the spherical coordinate system is used to generate glyph topology, Fig. 33.

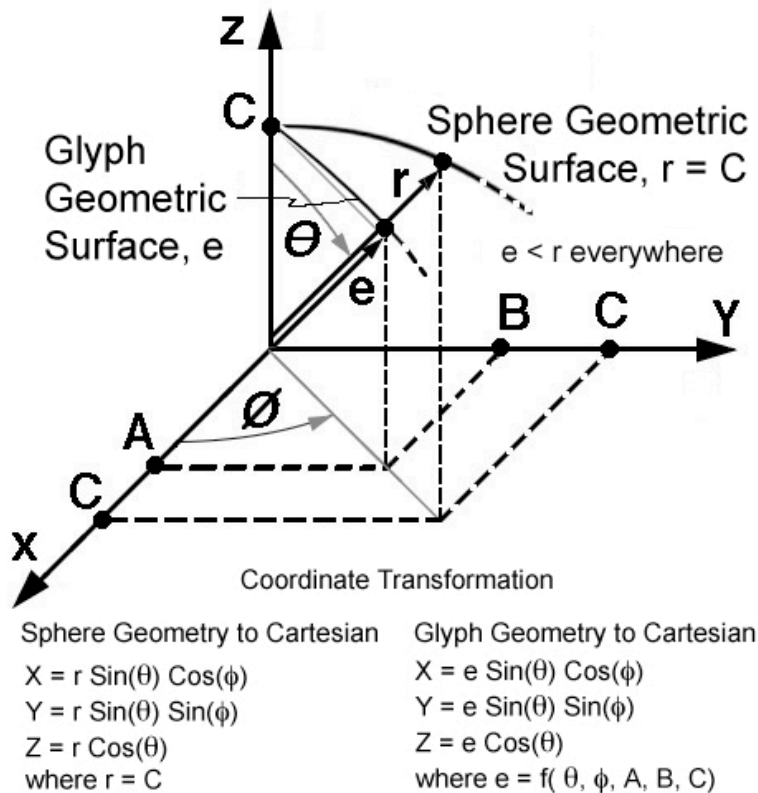


Figure 33. Spherical coordinate system used to generate glyph topology.

Depending on the glyph type the distance, e , is a function of the angles, θ and ϕ , and the components

of the second order stress tensor. For the quadric surface glyph this function is the function subroutine named sq, which is shown below as a code fragment. The value for sq is returned as the distance from the quadric surface to the geometric glyph centroid.

```

function sq(p,t,s11,s12,s13,s22,s23,s33)
c
c*****
c* Calculate distance, "sq", from the quadric surface to the geometric *
c* glyph centroid which is equivalent to the inverse of the square *
c* root of the normal stress of the first order stress tensor, Si, *
c* which acts in equilibrium with the second order stress tensor, Sij, *
c* defined by Cauchy's relations. In the direction defined by *
c* spherical coordinates: (theta,phi) *
c* where theta = t 0->180 degrees along the longitude *
c* phi = p 0->360 degrees along the latitude *
c*****
c
c Define unit vector direction cosines
d1=sin(t)*cos(p)
d2=sin(t)*sin(p)
d3=cos(t)
c
c Calculate components of the first order stress tensor from the
c second order stress tensor terms using Cauchy's relationship
s1=s11*d1+s12*d2+s13*d3
s2=s12*d1+s22*d2+s23*d3
s3=s13*d1+s23*d2+s33*d3
c
c Calculate the normal, "sn", component of the first order stress tensor
c projected in the direction of the unit normal perpendicular to the
c plane on which the first order stress tensor is acting.
sn=s1*d1+s2*d2+s3*d3
c
c Calcualte quadric surface distance, sq
trace=(1./abs(s11)+1./abs(s22)+1./abs(s33))/3.0
sq=sqrt(trace/abs(sn))
c write(6,12)sn,sq
if(sq.gt.3.2*trace)sq=3.2*trace
c 12 format(' *****
c *****',/, ' sn=',e12.5, ' sq=',e12.5)
c
return
end

```

When all of the principal stresses are positive the quadric surface is an ellipsoid, Fig. 32. When one or two of the principal stresses are negative the quadric surface is a symmetric three dimensional elliptic cone, Fig. 34. Because color gradients of stress type are distorted when mapped onto the irregular shapes of the conical quadric surfaces, Mercator maps of the stress type color gradient are seen undistorted below each image.

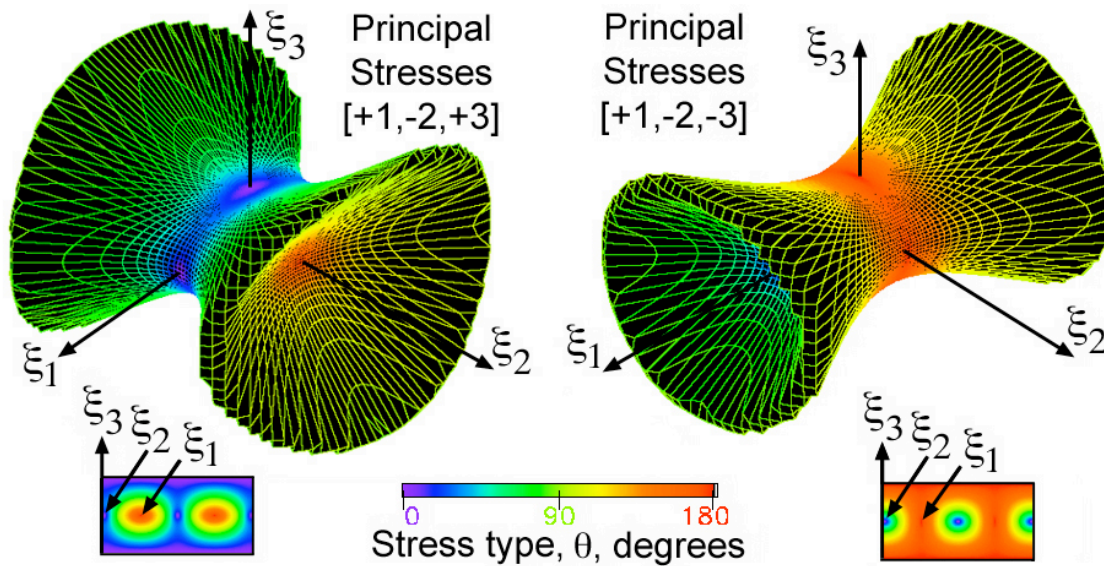


Figure 34. Stress quadric elliptical conical surface for [+1,-2,+3] and [+1,-2,-3]

These conical surfaces are interesting in that they clearly show the 3D curved surfaces along which pure shear exists. Returning to Fig. 28 the state of pure shear exists when $\sigma_N = 0$ on the plane (P_1, P_2, P_3) which is the same plane shown in Fig. 30. When the stress σ_i is parallel to the plane (P_1, P_2, P_3) and perpendicular to the unit vector, n_i , the quadric surface must extend to infinity along a collection of lines that define pure shear. This collection of lines form a conical shape, Fig. 34. Because these cones extend to infinity these glyphs must be truncated. After experimenting with different values for cutting off the distance PQ in Fig. 31, the following code segment, taken from the sq function subroutine, proved to yield acceptable results.

```

trace=(1./abs(s11)+1./abs(s22)+1./abs(s33))/3.0
sq=sqrt(trace/abs(sn))
if(sq.gt.3.2*trace)sq=3.2*trace
    
```

As expected the green color near pure shear is seen on the truncated portion of the glyphs shown in Fig. 34. Unfortunately the green color corresponding to pure shear at infinity has been truncated.

All tensor glyphs require a list of x, y, and z coordinates for each vertice located on the glyph surface and a list of vertices associates with each polygon that creates the glyph surface. The vertice list of x, y, and z coordinates is calculated from the distance return by the function subroutine associate with each type of second-order tensor glyph. However the polygon list of vertices is identically the same for all four second-order stress tensor glyphs developed in this section. The polygon list of vertices is generted by sequencing through the spherical coordinate angles θ and φ defined in Fig. 33 as shown in the code segment below.

```

program m_glyph_poly_tp
c
c*****
c program m_glyph_poly_tp generates polygon file or "connectivity" data*
c file assigning polygon numbers to vertice numbers. Together with each*
c of the vertice data files associated with PNS, HWY, Reynolds, and the*
c quadric glyph, this polygon data file defines each of the four Sij *
c second order stress tensor 3D glyph geometries. *
c*****
    
```

```

c
  open(6,file='tp_poly.out',status='unknown',err=8888)
  open(8,file='d_poly.dat',status='unknown',err=8888)
  pi=acos(-1.)
c
c 360 and 180 Resolution Divided by 3
  nphi=121
  rphi=360.0
  ntheta=61
  rtheta=180.0
c
c calculate the total number of vertices
  ivert=0
  do 200 iphi=1,nphi
  do 100 itheta=1,ntheta
  ivert=ivert+1
100 continue
200 continue
  write(6,210)ivert
210 format(' Total number of vertices=',i7)
c
c create polygonal portion of the wave surface topology
  ipnt1=0
  iarray=0
  nphm1=nphi-1
  nthm1=ntheta-1
  do 400 iphi=1,nphm1
  do 300 itheta=1,nthm1
  theta=(itheta-1)*rtheta/(nthm1-1)
  ipnt2=ipnt1+1
  ipnt4=ipnt1+ntheta
  ipnt3=ipnt4+1
  if (theta.eq.0.0)then
  n=3
  write(8,255)n,ipnt1,ipnt2,ipnt3
255 format(4(1x,i5))
  elseif (theta.eq.180.0)then
  n=3
  write(8,255)n,ipnt1,ipnt2,ipnt4
  else
  n=4
  write(8,260)n,ipnt1,ipnt2,ipnt3,ipnt4
260 format(5(1x,i5))
  endif
  iarray=iarray+n+1
  ipnt1=ipnt1+1
  ielmnt=ielmnt+1
300 continue
  ipnt1=ipnt1+1
400 continue
  write(6,500)iarray
500 format(' Total number of polygons=',i7)
c
8888 stop
  end

```

A complete summary of these examples with the code that was used to generate images of stress quadric glyphs and other glyph types are posted at:

http://www.jwave.vt.edu/~rkriz/Projects/Sij_glyphs/Sij_glyph_Example/ .

A visual summary of images (*.jpg), animations (animated *.gif), and VRML (*.wrl) files are posted at:

http://www.jwave.vt.edu/~rkriz/Projects/Sij_glyphs/Sij_glyph_Example/Results/Sij_results.html .

At the bottom right of the visual summary web page .../Sij_results.html composite images show the three quadric surface glyphs in Figs 32 and 34 together for comparison. Off diagonal stress tensor components for these three glyphs are zero and no rotations into a principal stress state are observed.

However the fourth glyph where $\sigma_{ij} = (\sigma_{11}, \sigma_{22}, \sigma_{33}, \sigma_{12}, \sigma_{13}, \sigma_{23}) = (-0.069e+03, -0.018e+03, +0.274e+03, -0.074e+03, +0.021e+03, -0.041e+03)$ is not in a principal stress state and a rotation into a principal stress state is observed: [VRML-1 file](#) / [VRML-2 file](#) . A screen capture of this VRML file comparing these four quadric surface glyphs is shown in Fig. 35.

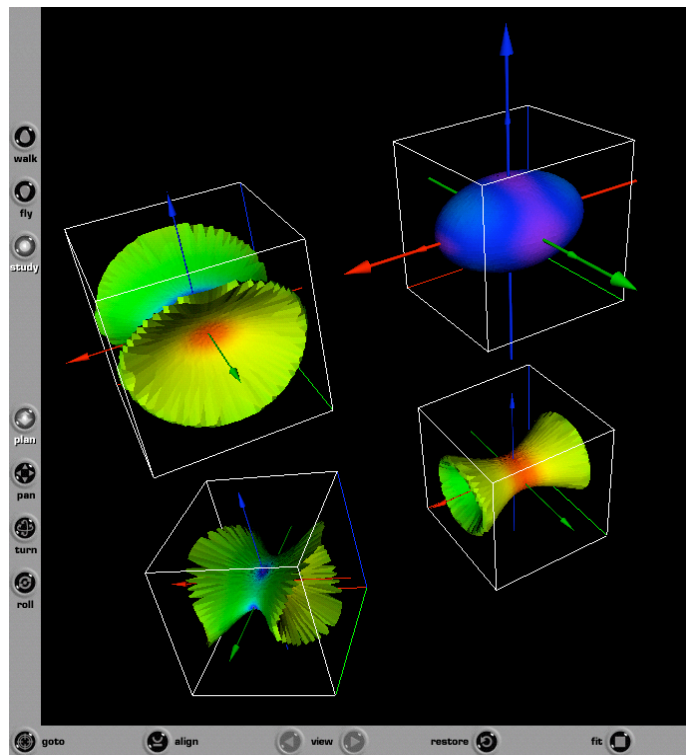


Figure 35. Screen capture of four second order stress tensor quadric surface glyphs as seen using the Cortona web browser plugin.

Each glyph is labeled with red, green, and blue axes which correspond to the ξ_1 , ξ_2 , and ξ_3 principal axes. Not all VRML web browser plugins can view fonts used to label these axes. To see the rotation of the fourth glyph a reference global axes is shown as larger red, green, and blue axes. The global reference axes is shown to coincide with the first quadric surface glyph, [+1,+2,+3] in the upper right corner in Fig. 35, because the center of the first glyph coincides with the origin of the global axes. Because the first quadric glyph is already in a principal stress state no rotation is observed and the axes coincide. However the fourth glyph shown in the lower left corner of Fig. 35 is observed to rotate with respect to the global reference axes. With VRML syntax it is also not possible to show a color legend that does not move with the global axes. Regardless of these issues, VRML files are useful because the viewer can rotate glyphs interactively and compare glyph shapes and orientations. If the reader does not have a VRML plugin installed on their web browser, animations of individual glyph rotations can be viewed using a standard web browser: select the movie icon shown to the right of each Mercator color

map. Larger clusters of glyphs would reveal more information, however the example shown here compares only four glyphs.

Haber Glyphs: Elliptical Disks and Rods ("keep it simple")

Haber [11] demonstrated how clusters of stress tensor glyphs in a 2D plane could be used to study the singular stresses in the region of a crack moving through a plate. Figure 36 shows an array of principal stress glyphs near one of two crack tips. Here a cluster of glyphs are overlaid on top of visual representations of two scalar properties: (1) square root of the kinetic energy density, which is plotted along the vertical axis and seen as a raised 2D surface plot above the cracked plate, and (2) log of the strain energy density, which is mapped as color on the raised surface plot of kinetic energy density. Hence the viewer can process several properties simultaneously as the crack moves through the plate. Viewing several physical properties simultaneously can be insightful.

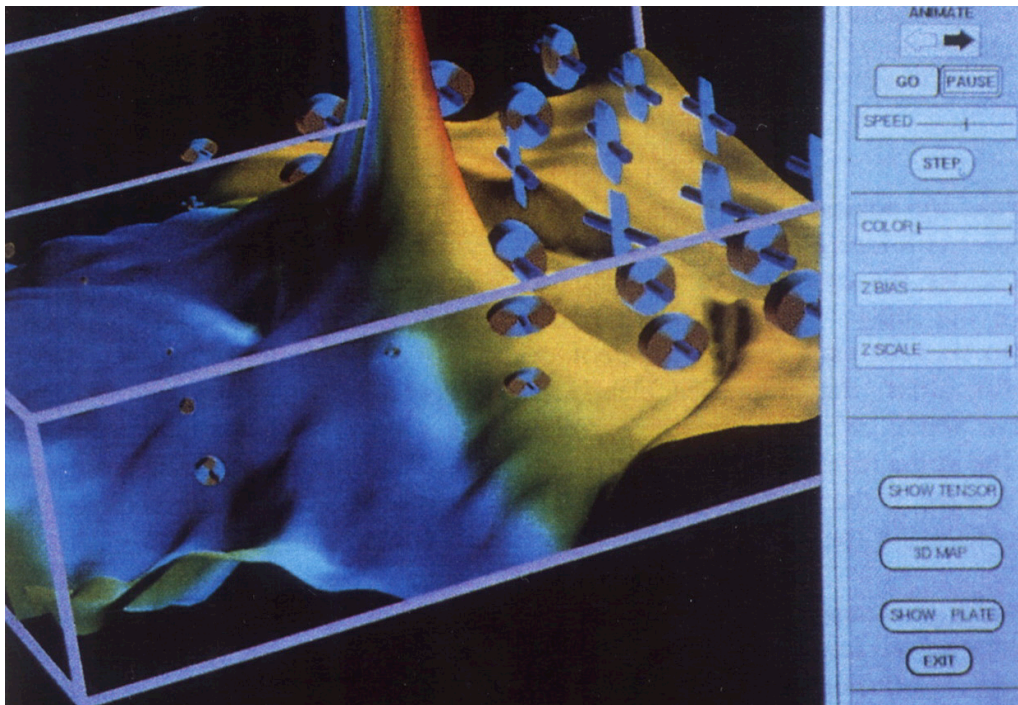


Figure 36. Cluster of Stress tensor glyphs showing the gradients of second order stress tensors uniformly distributed in the region near a moving crack and superposed on top of scalar properties shown here as gradients, Ref. [11]: surface height, sqrt(kinetic energy density) and color, ln(strain energy density).

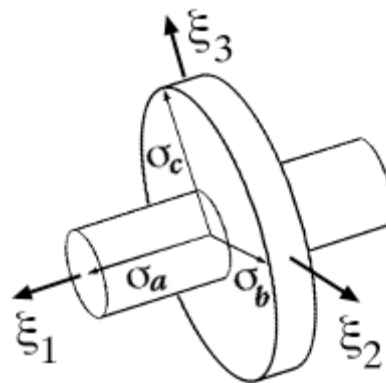


Figure 37. Haber stress tensor glyph.

Notice that unlike the quadric surface glyphs, this glyph's shape is that of a simple rod and an elliptical disk. Although the quadric surface reveals additional information about the direction of the stress vector in a particular direction, Haber's glyphs are better suited to reveal magnitudes of the principal stress state without obscuring other properties as shown in Fig. 36. In this case less is more when selecting a glyph type. The shape shown above, Fig. 37, is more easily recognized when envisioning eigenvalues or principal stresses as minor, intermediate, and major axes. Because of this simple shape it is also easier to envision the principal directions. Perhaps glyphs can have too much information assimilated into its shape, color, and orientation. Although the quadric surface glyph is insightful, insight like beauty is in the eye of the beholder. Ultimately the scientist must decide how to envision their data. This is why the most insightful visual models are created and customized by the scientists themselves. The same is true when constructing the mathematical model of the physical system being studied. In both cases insight is realized when the scientist creates both their own mathematical and visual models.

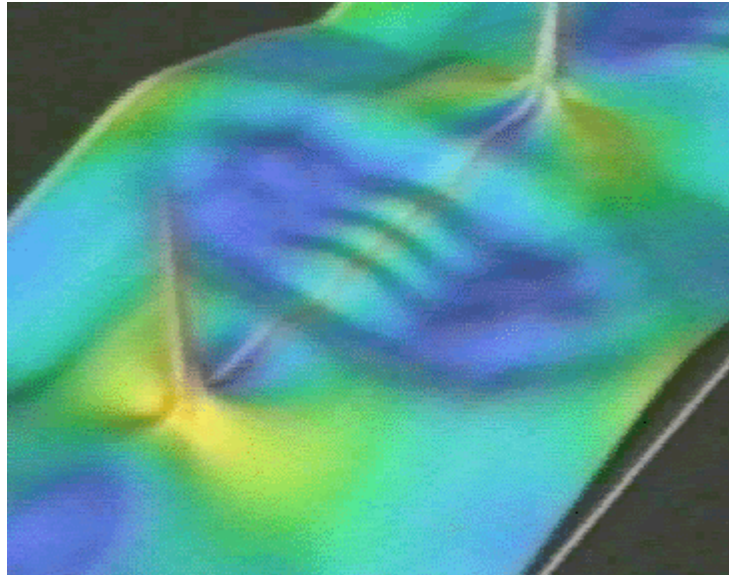


Fig. 38. Dynamic center crack: color represents $\log(\text{strain energy density})$, which is mapped onto a raised surface that represents the square root of the kinetic energy density. Notice the singularity at the crack tip, Ref. [12]. Animation: [MPEG Movie](#) (1.2Mb,141 frames)

An interference pattern observed at the center of a plate in Fig. 38 is caused by circular stress waves emanating from the two crack tips. Here the stress tensor glyphs have been removed to view the development of these interference patterns in an animated movie of Fig. 38, Ref. [12]. This animation displays the simulation - visualization results of two crack tips growing away from the center of the plate and shows the development of this interesting interference pattern. This stress wave interaction provided an insightful explanation of the irregularities observed in the dynamic crack tip stress intensity factors measured experimentally at the National Bureau of Standards.

The numerical solution to this fracture mechanics problem provided the raw data from which the stress tensor glyphs were created. Although these glyphs were observed to move over large distances with the crack tip, which is an Eulerian concept, it is interesting to note that the deformation field is not Eulerian but Lagrangian.

Reynolds Stress Tensor Glyphs: Normal Stresses Define Shape

Moore, Schorn and Moore [13] used Reynolds stresses to study turbulent flow. The stress tensor components are written here as a dyadic product which is equivalent to a tensor outer product of the

fluctuating velocities (u,v,w).

$$\overline{u_i u_j} = \begin{bmatrix} \overline{uu} & \overline{uv} & \overline{uw} \\ \overline{uv} & \overline{vv} & \overline{vw} \\ \overline{uw} & \overline{vw} & \overline{ww} \end{bmatrix} \quad (28)$$

Once the principal directions are determined, the principal components of the Reynolds stress tensor are found by transforming the fluctuating velocity components,

$$u_{Pn} = u P_{n,x} + v P_{n,y} + w P_{n,z} = u_i P_{n,i} \quad (29)$$

where the repeated indices "i" implies summation and the subscript "n" on P is not an index but implies principal directions. The dyadic product is used again to create the components of the Reynolds stress tensor but now in the principal stress state.

$$\overline{u_{Pn} u_{Pm}} = \overline{u_i u_j} P_{n,i} P_{m,j} \quad (30)$$

A new glyph can now be created by mapping this relationship into a cube with the unit vector (dx,dy,dz), where $\sqrt{dx^2 + dy^2 + dz^2} = 1$.

$$\begin{aligned} \overline{u_n^2} &= d_x^2 \overline{u^2} + d_y^2 \overline{v^2} + d_z^2 \overline{w^2} \\ &\quad + 2(d_x d_y \overline{uv} + d_y d_z \overline{vw} + d_x d_z \overline{uw}) \end{aligned} \quad (31)$$

As shown in Fig. 39 the resulting glyph is peanut shaped. Unlike the quadric surface the largest principal stress corresponds to the largest dimension and unlike the Haber glyph the exaggerated curvature of the peanut shape emphasizes the anisotropy of the normal component of the principal stress. To emphasize the shape of this glyph, Moore, Schorn and Moore [13] mapped color contours of minimum and maximum normal stress onto the glyph surface.

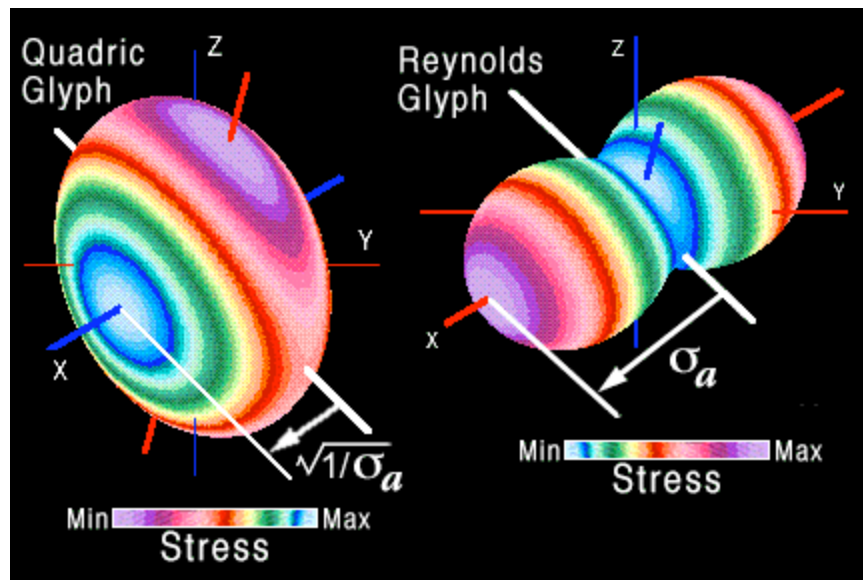


Figure 39. Comparison of the Reynolds stress tensor glyph with a quadric surface glyph, Ref. [13].

The comparison in Fig. 39 demonstrates that the principal stress σ_a along the X axis is scaled differently. For the quadric glyph, property (i) in Fig. 31 requires the distance from the geometric centroid to the surface equal the square root of $1/\sigma_a$. For the Reynolds glyph the distance from the geometric center to the surface is equal to σ_a . This reverses the maximum and minimum stresses mapped onto the surface. The same is true for the other principal stresses and their directions. The shape of the Reynolds glyph is constructed from the normal stress component, σ_N , of the first order tensor, σ_i in Fig. 28. However vectors acting normal to the quadric surface shows the direction of the first order tensor, σ_i . Each glyph envisions a different property of σ_i . The choice of which glyph to use depends on what property the researcher wants to investigate when envisioning information for insight or what property the research wants to use when presenting information to educate others. When envisioning information for presentation the rule is not to make the graphic too "busy" or cluttered with detail to the point of being distracting. When envisioning information for insight, the rule is to compare as many different properties as possible in the same space without reaching the researchers cognitive limit. Because everyone's limit is different, it is important that the researcher create their own graphical model and not leave this task up to information visualization experts who may not understand the science. The researcher is the expert when it comes their data.

When envisioning information for insight, more information is obtained when arranging these glyphs in an evenly spaced array, compared to a conventional use of contour lines and vectors, which is more popular for presentation. These two formats are compared in Fig. 40 which is a composite of Figs 2 and Fig. 8 taken from Ref. [13]. In the lower left region the glyph size is scaled to represent the magnitude of the principal stresses. The larger glyphs represent larger stresses which can obscure or hide information on adjacent glyphs.

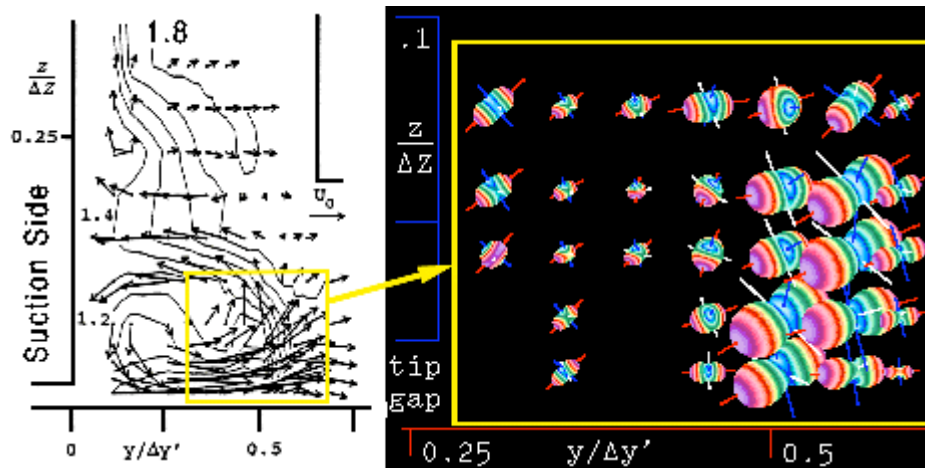


Figure 40. Comparison of Reynolds stress tensor glyphs with contour lines, Fig. 2 (left) and Fig. 8 (right) taken from Ref. [13]. A [larger format](#) of this figure is made available here and in Ref. [13].

The Reynolds and quadric glyphs are compared again, but using different color mapping proposed in Figs 28 and 31. The color contours mapped onto the surface in Figs 39 and 40 are scaled with respect to the minimum and maximum normal stresses which can be very useful for both insight and presentation. However if the researcher wants to envision the direction of the orientation of the first order stress tensor, σ_i , as a stress type, this choice is shown in Fig. 41. Again the point is made that envisioning information should be a choice within the intent to provide scientific insight or to educate others -- "presentation".

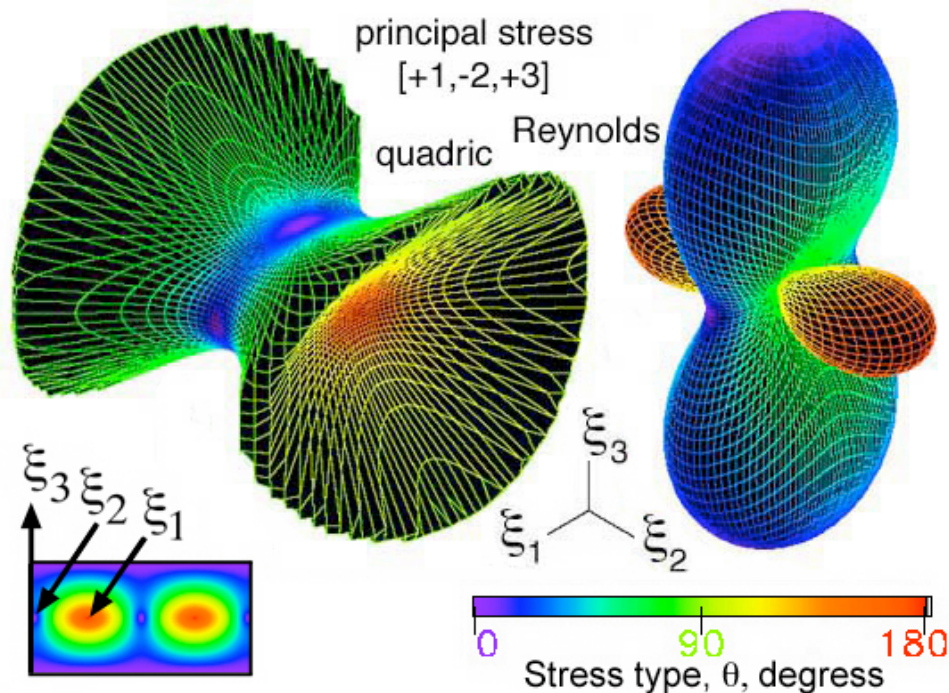


Figure 41. Comparison of Reynolds and quadric glyphs using a color gradient on the surface that shows stress type for a principal stress state of [+1,-2,+3].

By mapping stress type as color, the green shear stress is observed to coincide with the conical surface of the quadric glyph, where shear is expected, but shear is observed on the Reynolds glyph surface

where it was not expected. This new information reveals that although the shape of the Reynolds glyph is defined only by using the normal stress components, σ_N , shear stress can be envisioned as well. The distance from the centroid of the Reynolds glyph to the surface is calculated using the function subroutine, sn, shown below.

```

function sn(p,t,s11,s12,s13,s22,s23,s33)
c
c*****
c* Calculate normal component, "sn" of the first order stress tensor *
c* acting in the direction of the unit vector normal to the plane on *
c* which the first order stress tensor, Si, acts in equilibrium with *
c* the second order stress tensor, Sij, defined by Cauchy's relation. *
c* In the direction defined by spherical coordinates: (theta,phi) *
c* where theta = t 0->180 degrees along the longitude *
c* phi = p 0->360 degrees along the latitude *
c*****
c
c Define unit vector direction cosines
d1=sin(t)*cos(p)
d2=sin(t)*sin(p)
d3=cos(t)
c
c Calculate components of the first order stress tensor from the
c second order stress tensor terms` using Cauchy's relationship
s1=s11*d1+s12*d2+s13*d3
s2=s12*d1+s22*d2+s23*d3
s3=s13*d1+s23*d2+s33*d3
c
c Calculate the normal component, "sn" of first order stress tensor
c projected in the direction of the unit normal perpendicular to the
c plane on which the first order stress tensor is acting.
sn=s1*d1+s2*d2+s3*d3
c
return
end

```

A comparison similar to that done for different types of principal stress states in Fig. 35 is shown here for Reynolds glyphs in Fig. 42. Again the [VRML-1](#) and [VRML-2](#) files can be downloaded into a web plugin viewer or *.gif animated rotations of the same Reynolds glyphs can be viewed from movie icon links on the [Sij_results.html](#) web page.

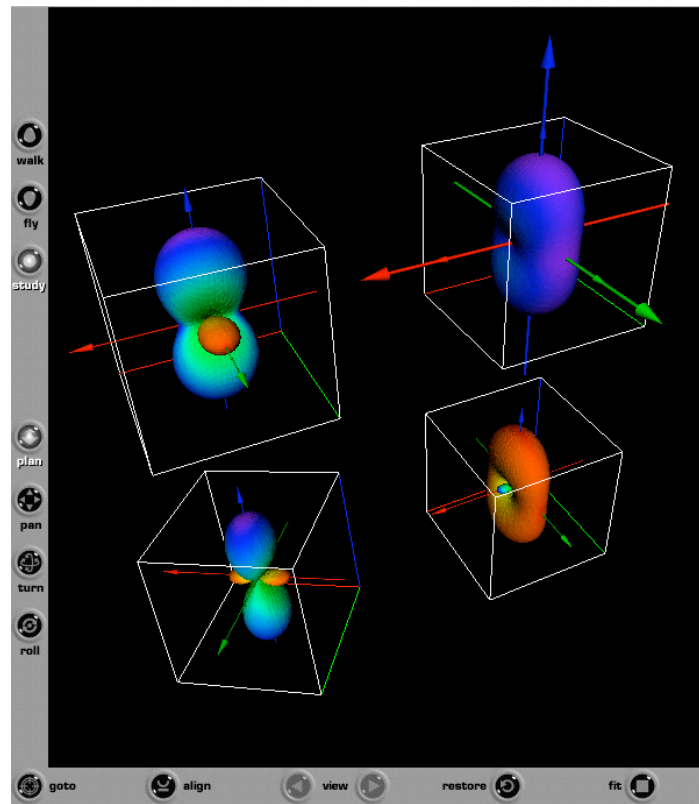


Figure 42. Screen capture of four second order stress tensor Reynolds glyphs as seen using the Cortona web browser plugin. Web links are provided for [VRML-1](#) and [VRML-2](#) files.

HWY Glyphs: Shear Stresses Define Shape

The HWY stress glyph is named in honor of its authors, Hashash, Wotring, and Yao [14], who emphasized envisioning the shear component, σ_S , of the first order stress tensor, σ_i shown in Fig. 28. The HWY glyph was developed for a geotechnical application where the shear component of the first order stress tensor was of interest. The quadric, Reynolds, and HWY glyphs are compared in Fig. 43 using the color mapping proposed in Figs. 28 and 31.

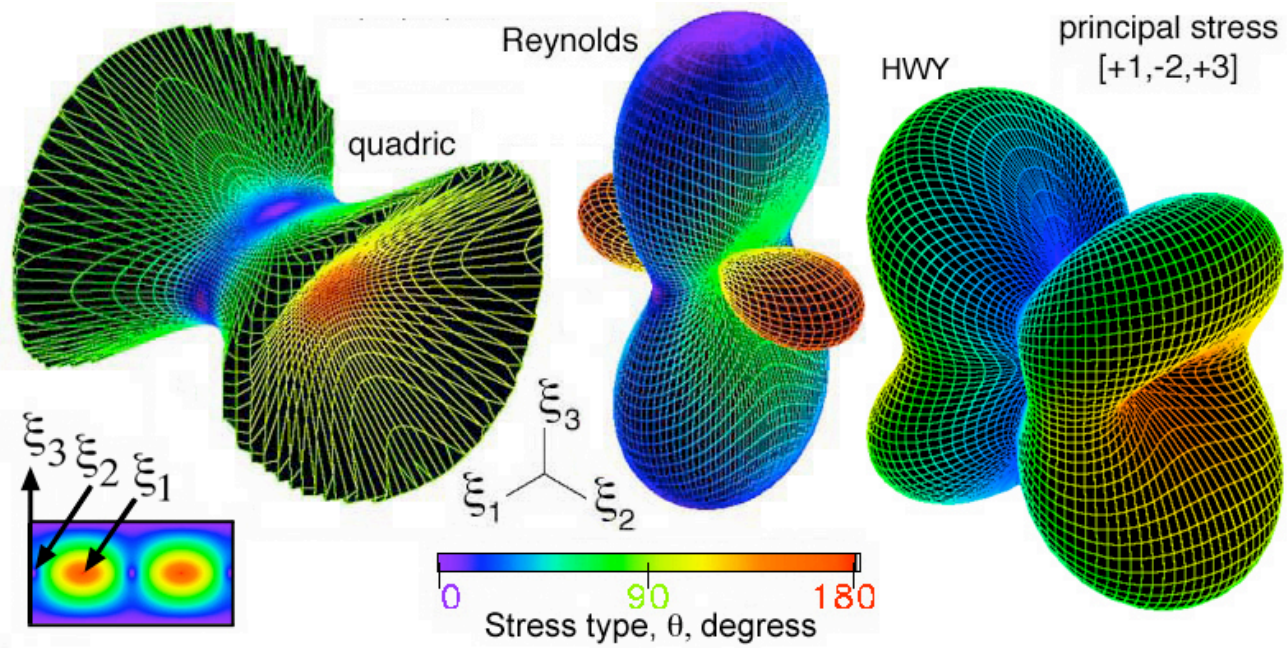


Figure 43. Comparison of quadric, Reynolds and HWY glyphs using a color gradient on the surface that shows stress type for a principal stress state of $[+1, -2, +3]$.

The distance from the centroid of the HWY glyph to the surface is the shear component of the first order stress, σ_i , shown in Fig. 28. This shear component is calculated using the function subroutine, `ss`, shown below.

```

function ss(p,t,s11,s12,s13,s22,s23,s33)
c
c*****
c* Calculate shear component, "ss", of the first order stress tensor *
c* acting in the direction of the unit vector normal to the plane on *
c* which the first order stress tensor,  $S_i$ , acts in equilibrium with *
c* the second order stress tensor,  $S_{ij}$ , defined by Cauchy's relation. *
c* In the direction defined by spherical coordinates: (theta,phi) *
c* where theta = t 0->180 degrees along the longitude *
c*      phi = p 0->360 degrees along the latitude *
c*****
c
c Define unit vector direction cosines
  d1=sin(t)*cos(p)
  d2=sin(t)*sin(p)
  d3=cos(t)
c
c Calculate components of the first order stress tensor from the
c second order stress tensor terms using Cauchy's relationship
  s1=s11*d1+s12*d2+s13*d3
  s2=s12*d1+s22*d2+s23*d3
  s3=s13*d1+s23*d2+s33*d3
c
c Calculate the normal, "sn" component of first order stress tensor
c projected in the direction of the unit normal perpendicular to the
c plane on which the first order stress tensor is acting.
  sn=s1*d1+s2*d2+s3*d3
c

```

```

c Calculate the shear "ss" component
  ss=sqrt(s1**2+s2**2+s3**2-sn**2)
c
  return
end

```

A comparison similar to that done for different types of principal stress states in Fig.s 35 and 42 is shown here for HWY glyphs in Fig. 44. Again the [VRML-1](#) and [VRML-2](#) files can be download into a web plugin viewer or *.gif animated rotations of the same HWY glyphs can be viewed from movie icon links on the [Sij_results.html](#) web page.

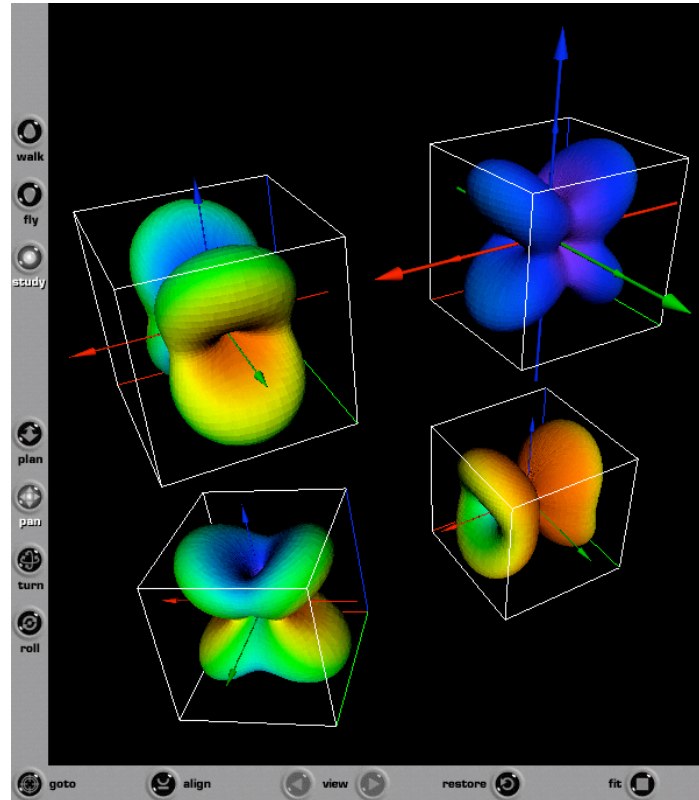


Figure 44. Screen capture of four second order stress tensor HWY glyphs as seen using the Cortona web browser plugin. Web links are provided for [VRML-1](#) and [VRML-2](#) files.

PNS glyph: Principal Normal Stresses Define Ellipsoidal Shape

Unlike the Quadric, Reynolds, and HWY glyphs, the PNS glyph is always an ellipsoid whose major, intermediate, and major axes corresponds to the Principal Normal Stresses (PNS) ($\sigma_a, \sigma_b, \sigma_c$). The PNS glyph was developed by M. Yaman and R.D. Kriz where the intent was to keep the glyph shape simple like the Haber glyph, but unlike the Haber glyph provide additional informaton of the stress type as color mapped onto the PNS glyph surface. The quadric, Reynolds, HWY, and PNS glyphs are compared in Fig. 45 using the color mapping proposed in Fig.s 28 and 31.

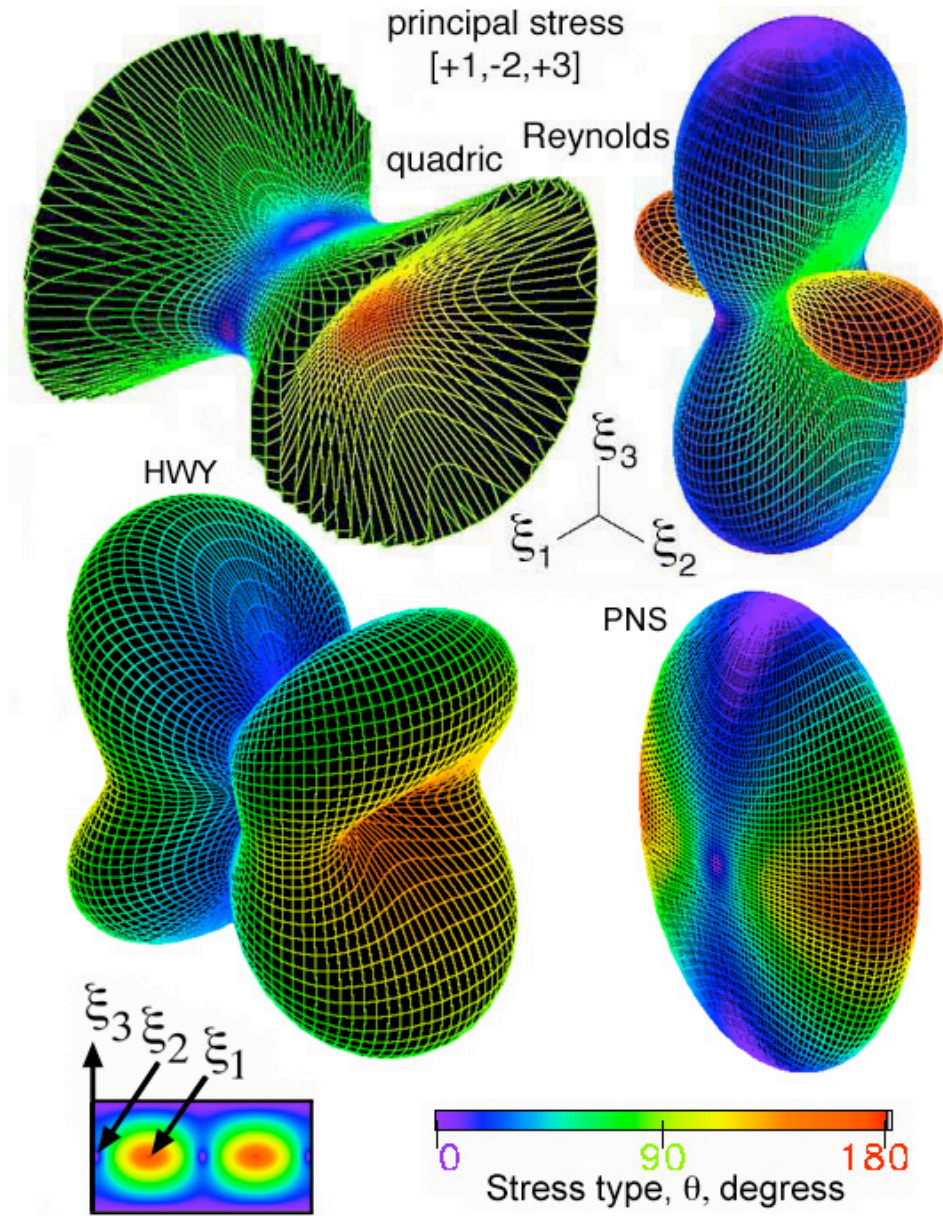


Figure 45. Comparison of quadric, Reynolds, HWY, and PNS glyphs using a color gradient on the surface that shows stress type for a principal stress state of [+1,-2,+3].

The distance from the centroid of the PNS glyph to the surface of an ellipsoid whose major, intermediate, and minor axis are defined by the principal stresses ($\sigma_a, \sigma_b, \sigma_c$). This distance is returned as a radius, e , and calculated using the function subroutine, e , shown below.

```

function e(p,t,a,b,c)
c
c*****
c* Calculate radius, e, for an ellipsoid whose major, intermediate, *
c* and minor axis are given by a,b,c respectively, in the direction *
c* defined by spherical coordinates: (theta,phi). *
c* where theta = t 0->180 degrees along the longitude *
c* phi = p 0->360 degrees along the latitude *

```

```

c*****
ct2=cos(t)*cos(t)
st2=sin(t)*sin(t)
cp2=cos(p)*cos(p)
sp2=sin(p)*sin(p)
d=st2*cp2/a**2+st2*sp2/b**2+ct2/c**2
e=sqrt(1/d)
return
end

```

A comparison similar to that done for different types of principal stress states in Fig.s 35, 42, and 44 is shown here for PNS glyphs in Fig. 46. Again the [VRML-1](#) and [VRML-2](#) files can be download into a web plugin viewer or *.gif animated rotations of the same PNS glyphs can be viewed from movie icon links on the [Sij_results.html](#) web page.

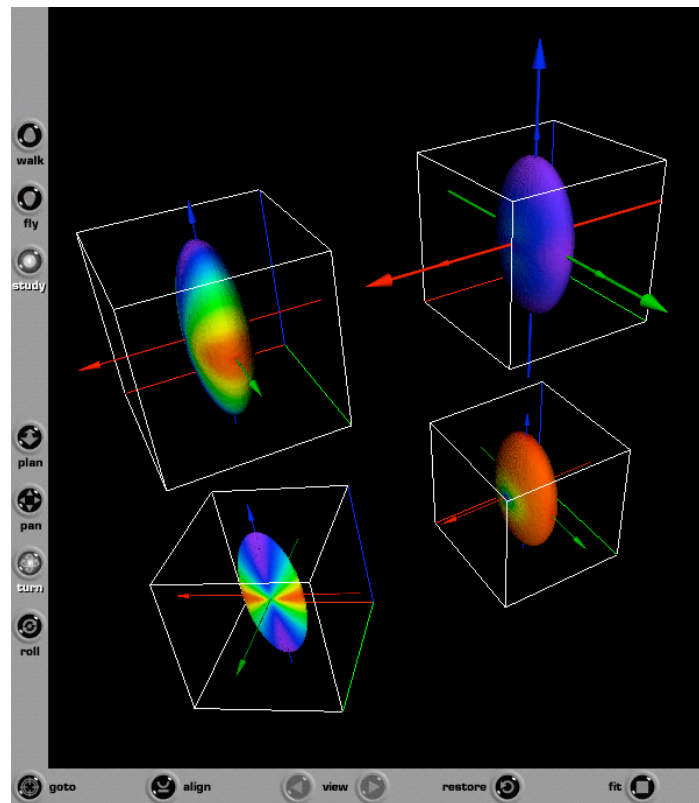
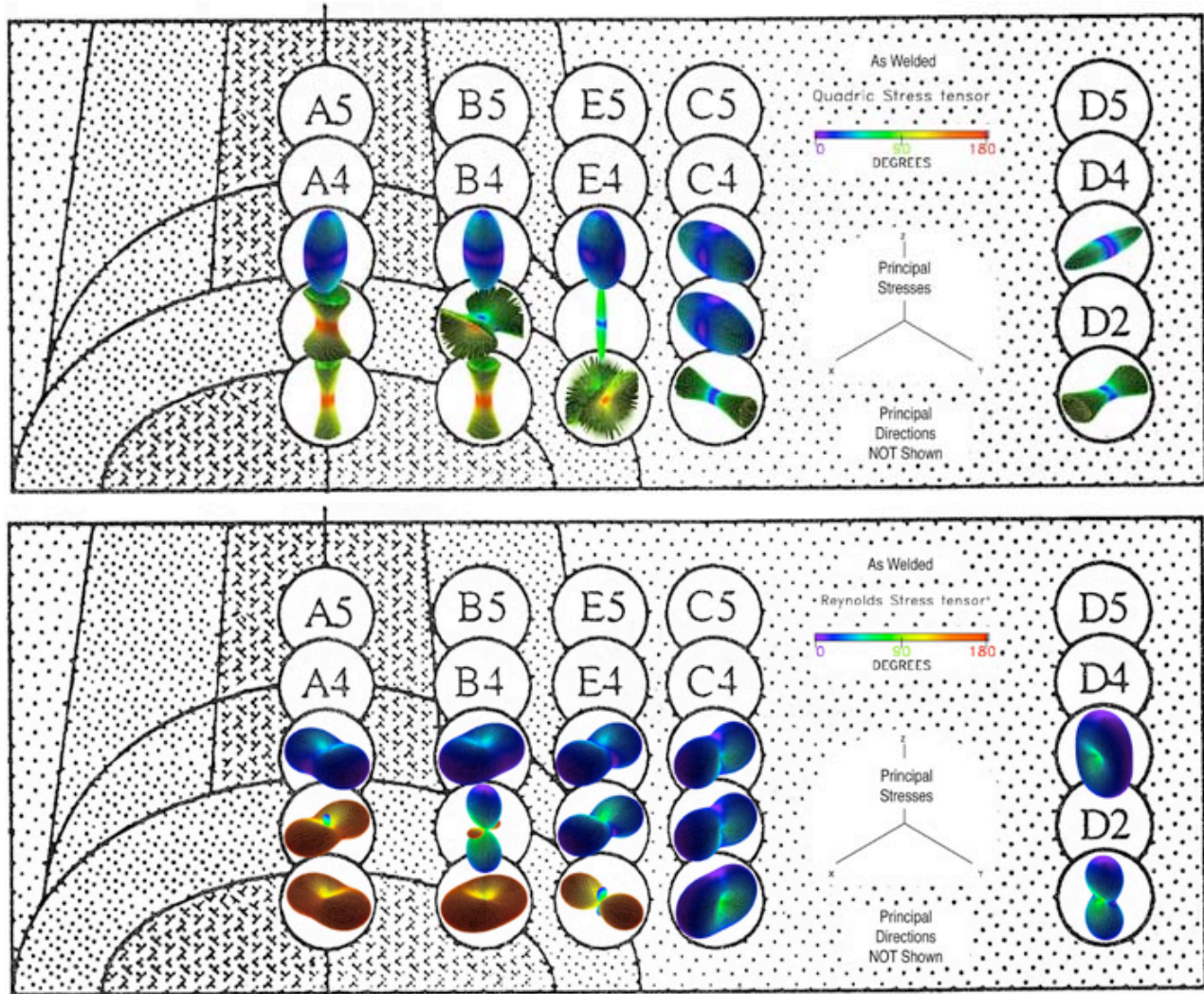


Figure 46. Screen capture of four second order stress tensor PNS glyphs as seen using the Cortona web browser plugin. Web links are provided for [VRML-1](#) and [VRML-2](#) files.

A visual summary of these four glyphs were used to study two different types of residual stresses gradients: 1) residual stresses near welds, and 2) surface residual stresses induced by plastic deformations (shot peening) in a Titanium alloy (Ti-6Al-4V). This research was collaboration with Professor M. Harting, and Mr. Mecit Yaman, Ph.D candidate, in the Department of Physics at the University of Cape Town, South Africa and Dr. Ron Kriz, Department of Engineering Science and Mechanics, Virginia Tech, Blacksburg, Virginia, USA. A complete description of results from this collaboration is available by going to the web link: [Residual Stress Gradient Visualization](#). However a brief summary is include here as an example of how an array of second-order stress tensor glyphs can be used to study residual stresses in welds and stress gradients near surfaces due to plastic deformation.

The first four images show the quadric, Reynolds, HWY, and PNS glyphs superposed on top of the

weld structure, Fig. 47. Only the principal stresses are shown in Fig. 47, which does not show the rotations into the principal stress state. Images in Fig. 47 are scaled to fit the width of a typical web page. To view these images in more detail, a [web link of results](#) in a larger image format is provided here for reference. For comparison only the quadric glyph type for "as-welded" and "post-heat-treated" are shown in one file where the rotations of the various principal stress states can be compared using the VRML file format, Fig. 48.



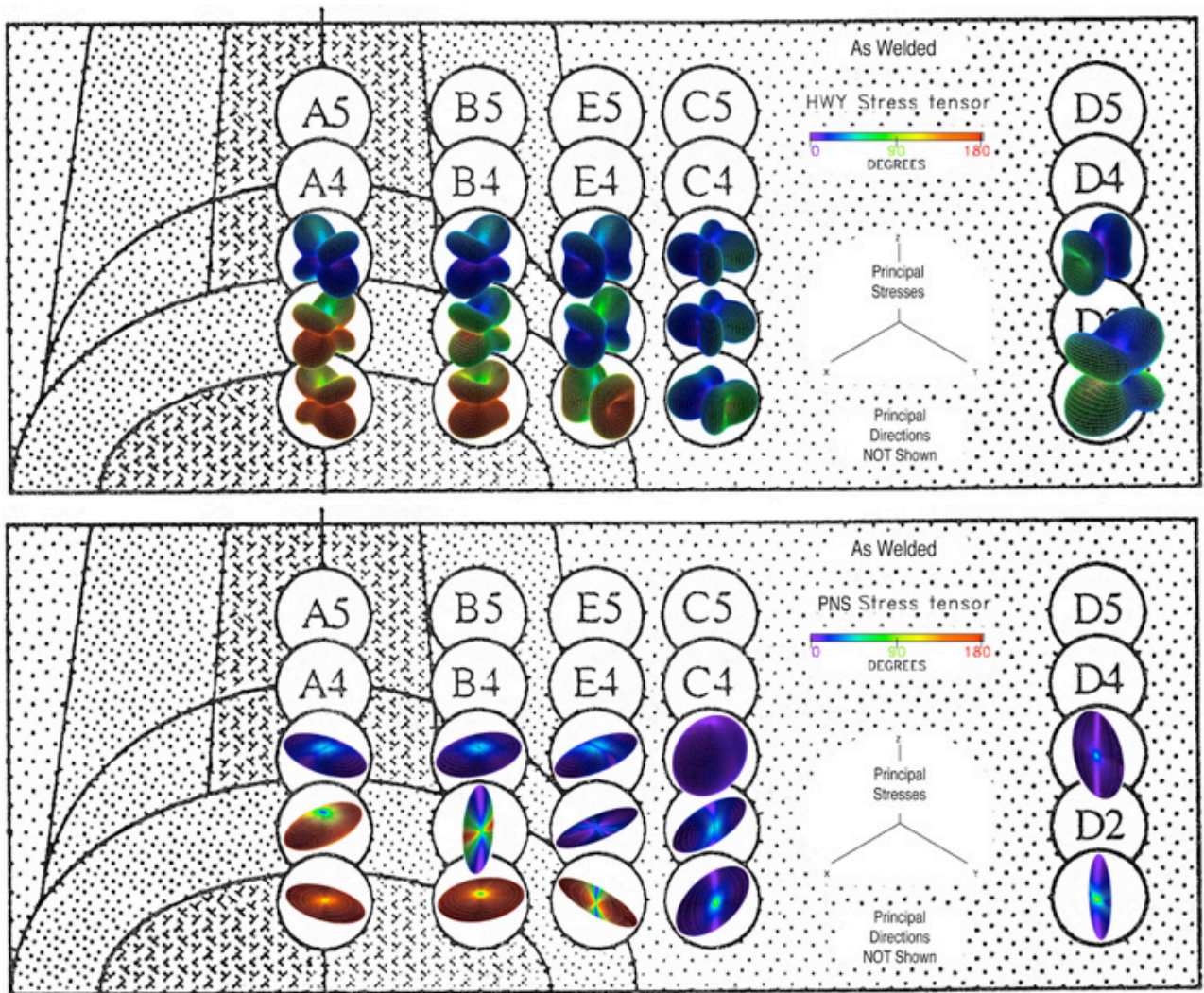


Figure 47. Quadric, Reynolds, HWY, and PNS glyphs for the "as-welded" condition is superposed onto weld structure. The "post-heat-treated" condition not shown A [web link of all results](#) including large image formats is provided here for reference.

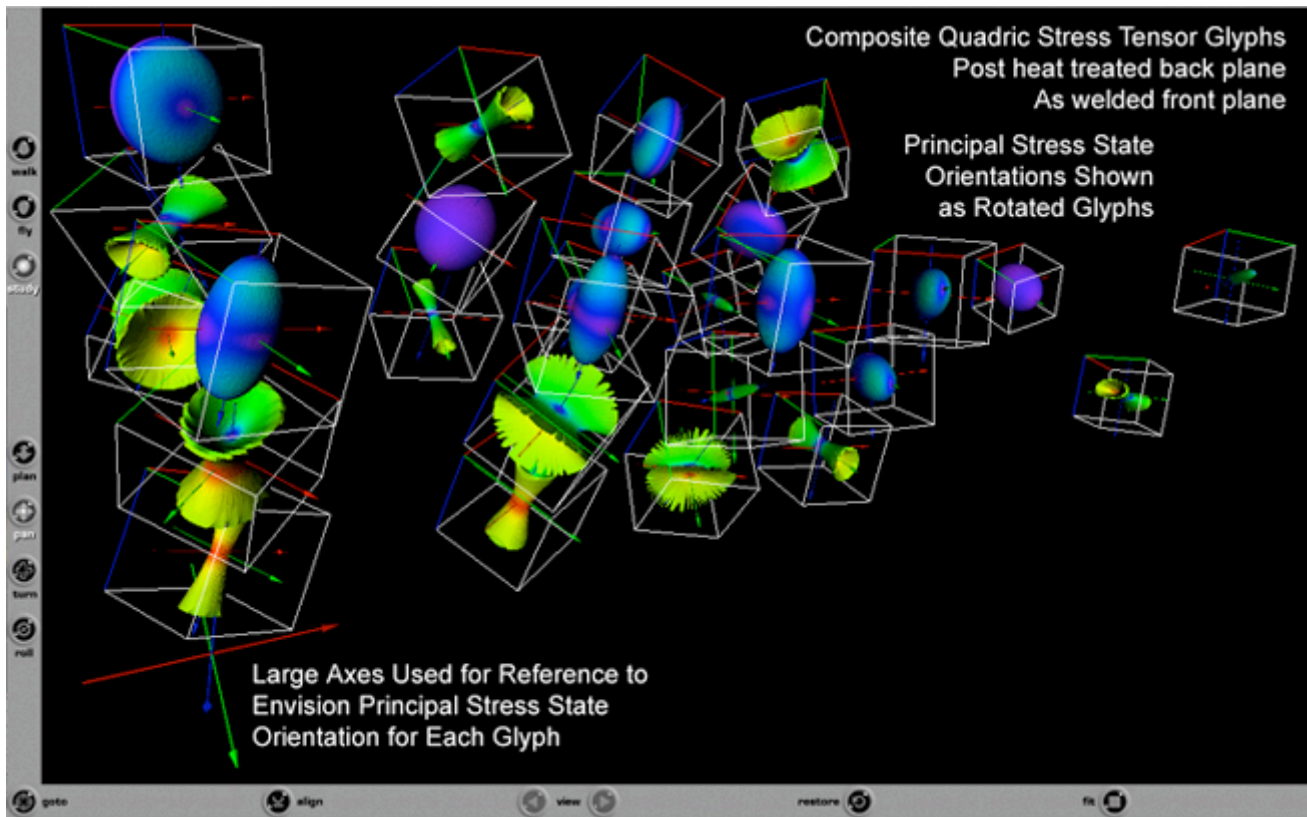


Figure 48. Quadric glyph arrays of "as-welded" and "post-heat-treated" combined into single [VRML-1](#) and [VRML-2](#) file format where principal directions are shown as rotated glyphs.

This collection of second-order stress tensor glyphs when organized into an array and superposed on top of the weld structures can facilitate the analysis of how changes in residual stresses correspond to weld structure. In Fig. 48 results in the "as-welded" conditions are observed to change when compared with the "post-heat-treated" condition. This large array of glyphs shown in Fig. 48 would benefit from an immersive virtual environment, where the viewer can move through space and view these stress tensor gradients immersively by using three-dimensional head tracking. This is possible by renaming the VRML-1 file extension from *.wrl to the Inventor format *.iv. This is possible because when SGI was the leader in graphical interface, the VRML-1 and Inventor file formats were interchangeable. Since most immersive application programming interfaces (APIs) can load Inventor files, the VRML-1 files can be viewed interactively both at the desktop computer using a Web browser plugin and in an immersive environment. Immersive environments are particularly useful when interpreting large arrays of data in a three-dimensional gradient format.

Briefly, results of stress gradients are also shown near a surface induced by plastic deformation (shot peening) in a Titanium alloy. Again web links to [VRML file formats](#) are provided for downloading into Web browser plugins or into immersive environments. A [web link of results](#) summarizes gradients near the surface where quadric, Reynolds, HWY, and PNS glyphs are used for comparison.

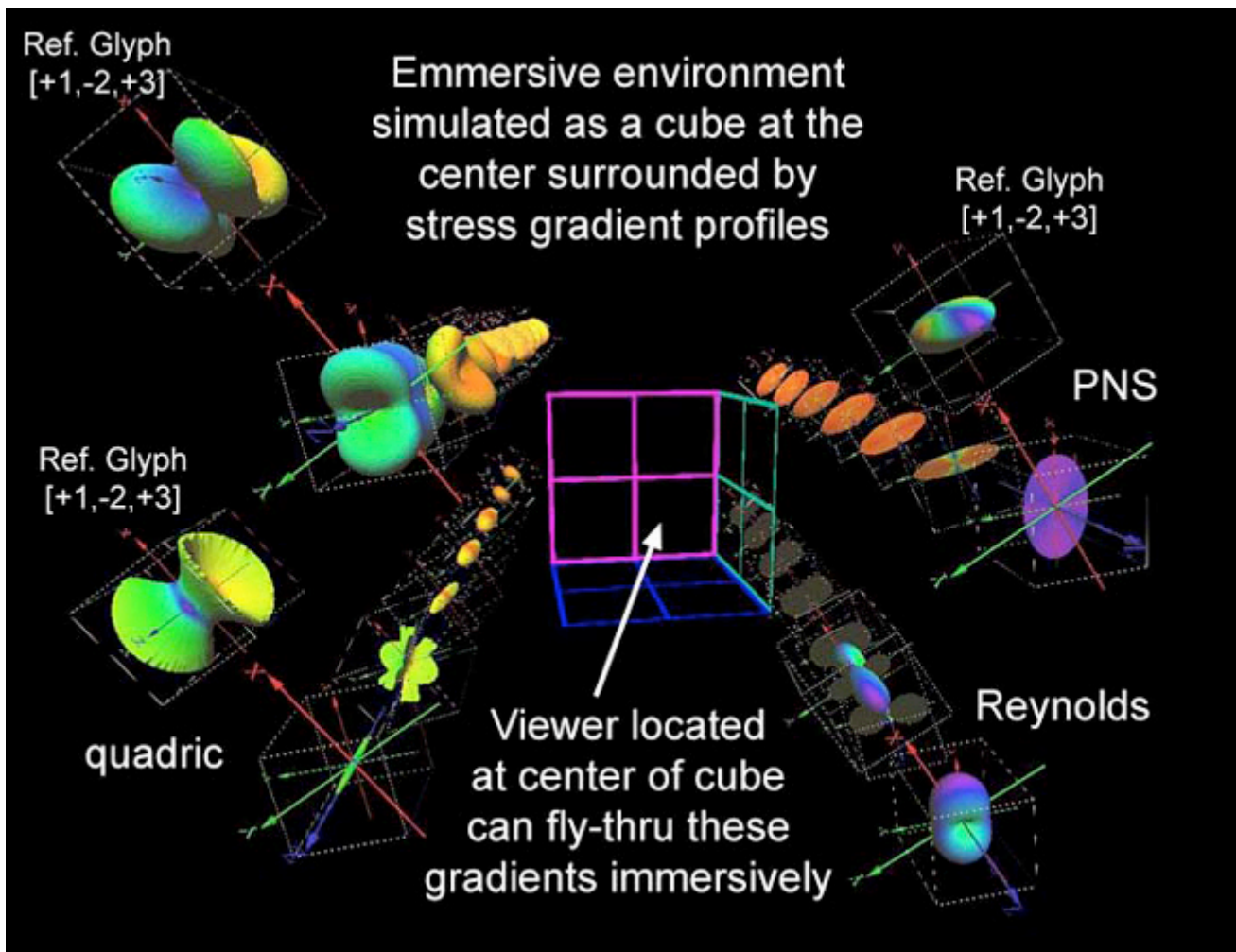


Figure 50. Residual stress profiles loaded into an immersive environment where the cube shown at the center visually simulates the location of the 10' by 10' by 10' walls where stereo images are projected.

These results show a significant change in the principal stresses near the surface, but only a slight rotational gradient with depth in both Fig.s 49 and 50. Immersive environments proved to be useful when large arrays of glyphs were created.

Second-Order Stress Tensor Gradients

Stress Tensor Gradients in One Dimension: Tensor Tubes

Many problems in continuum mechanics emphasize continuous changes in tensor properties: such as the comoving derivative of a property associated with a fluid particle moving through a fluid in Eulerian space or continuous lines of principal stress in a solid where the deformation field is defined in Lagrangian space. In the Haber glyph example clusters of stress tensors were used to envision a stress gradient near a crack tip in Lagrangian space. However when this same array of stress glyphs moved with the crack tip, these stress gradients were envisioned to change as they moved through space, which is an Eulerian concept. This regularly spaced array of Haber glyphs shown in Fig. 36 must be spaced so as not to obscure the isosurfaces of kinetic energy density and color gradients of strain energy density. Unfortunately there is a large stress gradient near crack tips, which requires closer spacing of stress tensor glyphs to accurately recover the gradient in this region. These are conflicting issues that can be

resolved by creating continuous stress tensor tubes.

Delmarcelle, Hesselink and Helman [15, 16] envisioned continuous changes of second order tensor fields as a stress tensor tube. Stress tensor tubes are an extension of the Haber glyph, where the perimeter of the Haber glyph (σ_b, σ_c) is used to create the tube's surface and the length of the rod (σ_a) is mapped as color onto the perimeter. This technique is used to envision very small changes in the second order stress tensor corresponding to small changes in distance, ΔX_3 . The components ($\sigma_a, \sigma_b, \sigma_c$) used to construct the tube can also be envisioned as the major, intermediate, and minor axes of the PNS stress tensor ellipsoid, Fig. 51. Here the minor axes, σ_c is used to map color on the perimeter.

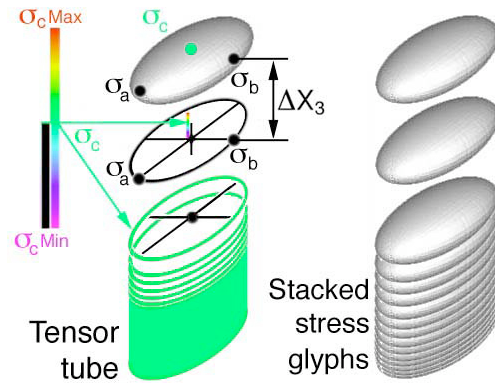


Figure 51. Creation of stress tensor tubes from stacked PNS ellipsoidal glyphs.

In Fig. 52 the center of the two glyph tubes propagate upward along trajectories or lines s that represent the direction (eigenvector) of the largest compressive stress. In this figure the color represents the magnitude of the largest compressive stress (the minor eigenvalue). The shape of the tube represents the magnitudes of the other two eigenvalues. Similar trajectories near the bottom of the figure for the other two eigenvectors take a shape that is everywhere perpendicular to the most compressive stress. These flat tened tubes show that one of the eigenvalues must be close to zero.

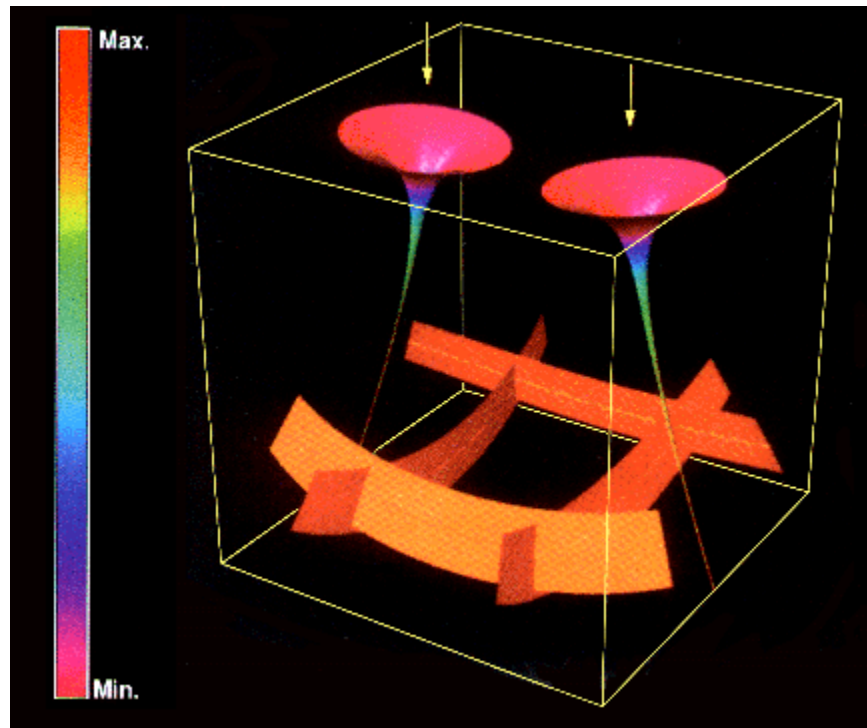


Figure 52. Elastic-stress tensor field in a solid induced by two compressive forces applied at the top surface, Refs. [15, 16].

The next figure, Fig. 53, shows how the shape of the tubes in Fig. 52 change if an additional tension force is applied at the top surface (the exact location is not specified) Ref. [15, 16]. The shape of these glyphs are shown to change with increasing tension force (a) -> (b) -> (c) -> (d).

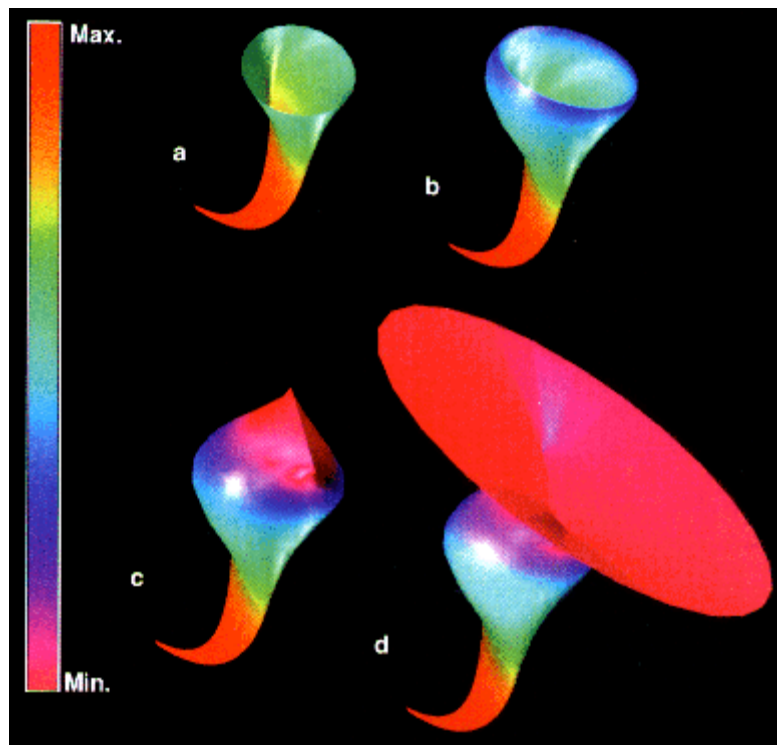


Figure 53. Elastic-stress tensor field glyphs shape changed by additional tension surface force. Glyph (c) shows that one of the principal stress is zero, Refs. [15, 16]

In this example the magnitude of the compressive principal stress was mapped as color on the continuous stress tensor glyph. Many other combinations are discussed in Ref. [15,16].

Tensor tubes prove to be useful when envisioning gradients in one direction: e.g. in Fig. 51 as ΔX_3 approaches zero the stacked PNS ellipsoidal glyphs obscure informaton in the X_3 direction, however color can be used to recover this information but only in X_3 direction. Since mathematical concept of gradients is three-dimensional, another visual approach is explored that envisions gradients of stress tensors in all three-dimensions.

Point Stress Tensor Gradients in Three Dimensions

Gradients of second order stress tensors in three-dimensions can be envisioned by drawing a collection of evenly space stress tensor glyphs in RCC space. Either quadric, Haber, HWY, or PNS glyphs can be used, however in Fig. 54 the PNS ellipsoidal glyph is used for similiticy. The center PNS glyph is used as the reference glyph and the surrounding PNS glyphs are located at evenly spaced distances, ΔX_1 , ΔX_2 , and ΔX_3 , which would be seen as a collection of glyphs located to the north, south, east, west, front, and back of the center glyph, Fig. 54.

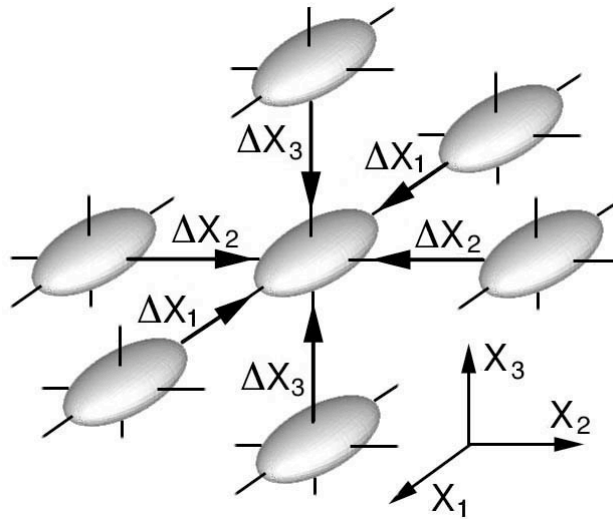


Figure 54. Stress glyph gradient where there is no change in shape or orientation of the nearest neighboring stress glyphs collapsing onto the center glyph.

If the glyph spacing is small but the 3D collection of glyphs does not obscure the viewer from seeing how glyphs change their shape and orientation as these glyphs collapse onto the center glyph, than the viewer is seeing a stress gradient within a discrete change in space.

$$\Delta\sigma_{ij} / \Delta x_k \quad (32)$$

In the limit as ΔX_k goes to zero, Eqn. (32) reduces to

$$\sigma_{ij,k} \quad (33)$$

which transforms as a third order tensor. Summing forces requires a contraction on the "i" and "k" indices which yields,

$$\sigma_{kj,k} \quad (34)$$

Comparing Eqn. (34) with equilibrium equation, $\sigma_{ji,j} = 0$, suggests that it may be possible to envision the stress state of static force equilibrium as a 3D gradient, but only if the viewer can visually confirm that Eqn. (34) sums to zero, on indice "k". Since the stress glyphs shown in Fig. 54 are all the same, the gradient, $\sigma_{ij,i}$, for this case is indeed zero. However if the stress glyphs surrounding the center glyph all have different shapes and orientations, then it is debatable if the observer can envision how the summation, $\sigma_{kj,k}$, goes to zero. However any gradient in Fig. 54 does indeed visually represent force equilibrium but only in the limit as ΔX_k goes to zero. This limiting process could be more accurately envisioned as animation where surrounding glyphs shape, color and orientation change as they collapse onto the center glyph. It is not difficult to extend this visual method to include time, which would than visually represent a commoving derivative of stress with respect to space and `time.

The collection of glyphs in Fig. 54 envisions the gradient collapsing or expanding on the center glyph but only for one particular orientation, $\sigma_{ji,j}=0$, which satisfies equilibrium in this particular direction. However equilibrium is a law, therefore it must exist in all possible directions and arbitrarily so. This idea of invariance in a physical sense is the same as invariance in a mathematical sense by transforming each term in the equilibrium equation, $\sigma'_{kj,k}=0$. The apostrophy symbolically represents this arbitrary mathematical transformation. The fact that the equation maintains it's form after such an arbitrary transformation is the idea of mathematical invariance. How would we envision a collection of glyphs that would visually represent a gradient in any arbitrary direction? What would this 3D image look like? One possible implementation of this idea is to envision an infinite set of stress quadric surface glyphs propagating outward from the center glyph in all possible directions simultaneously. This collection of stress tensor glyphs would be expanding not collapsing. This idea is similar to Huygen's principle for 2D plane waves emanating from a point, but using 3D stress quadric surface glyphs instead. A moving 3D small multiple of 3D objects. This image would be difficult to envision and represents a limit in our visual cognitive ability to envision stress gradients in any arbitrary direction. Although difficult for mortals to envision, such a surface would be seen as symmetric to satisfy equilibrium and it's gradients.

Envisioning Fourth-Order Stiffness Tensors, C_{ijkl}

Glyphs can also be used to better understand higher order tensors. For example, fourth order stiffness tensor, C_{ijkl} , can also be envisioned using simple glyphs. The fourth order stiffness tensor relates all of the components of the second-order strain tensor, l_{kl} to the second-order stress tensor, σ_{ij} .

$$\sigma_{ij} = c_{ijkl} \epsilon_{kl} \quad (35)$$

This relationship is called generalized Hooke's law. This equation is a tensor equation and can not be written in matrix notation unless using contracted Voigt notation. This contracted format is written as 6x6 matrice, however these contract terms will not transform as tensor components. Here the tensor format is maintain that will prove useful when envisioning physical properties associated with mathematical invariance of tensor equations. This mathematic invariance can be demonstrated when each term of the tensor Eqn. (36) is transformed as a tensor of that order and the original form of the tensor equation remains unchanged. When Eqn. (35) is combinded with the equations of motion, the result is another tensor equation called the Christoffel's equations of motion, Eqn. (36). A complete development of Christoffel's equations can be studied at: [Introduction to Mechanical Behavior of Anisotropic Materials: Geometric Representations of Elastic Anisotropy: All Tensor Components, \$C_{ijkl}\$](#) .

$$[C_{ijkl} v_i v_j - \rho v^2 \delta_{kl}] p_k = 0 \quad (36)$$

If the indices are expanded, Eqn. (36) reduces to eigen-value problem, where the eigenvalues, ρv^2 , are related to the wave speeds, v , and density, ρ , and the eigenvectors are the particle vibration directions, p_k , of Eqn. (36). The surface shown in Fig. 55 is generated by prescribing all possible directions, \mathbf{V}_i and \mathbf{V}_j in Eqn. (36) and mapping out all of these solutions as a glyph: the eigen-value solutions, wave velocities, v , is the distance from the geomtric center to the surface and the eigen-vector solutions are used to map a color for each eigen-value solution at the point where the pointing vector, \mathbf{V}_i , intersects the surface. Since both the eigen-values and their corresponding eigen-vectors are functions only of C_{ijkl} , see Eqn. (36), then the surface shape and colors shown in Fig. 55 can be used to envision this fourth-order stiffness tensor. Because all terms of the fourth-order tensor were used to calculate the wave surface and its colors we see the relationship between the eigenvalues and their corresponding eigenvectors at every point on this surface. We can also observe the spin properties of the displacement fields as color gradients that exist near degeneracies in the eigen-values that appear as the concave portion of the wave surface that collapse to a point (see black region). It is through these degeneracies that wave surfaces can interconnect into single continuous connected wave surfaces ([mode-transitions at eigen-value degeneracies](#)) Kriz and Ledbetter [18]. At these same degeneracies internal conical refraction exist. Again the mathematical invariant property of tensor equations is used here to develop an understanding of the physical properties envisioned in Fig. 55.

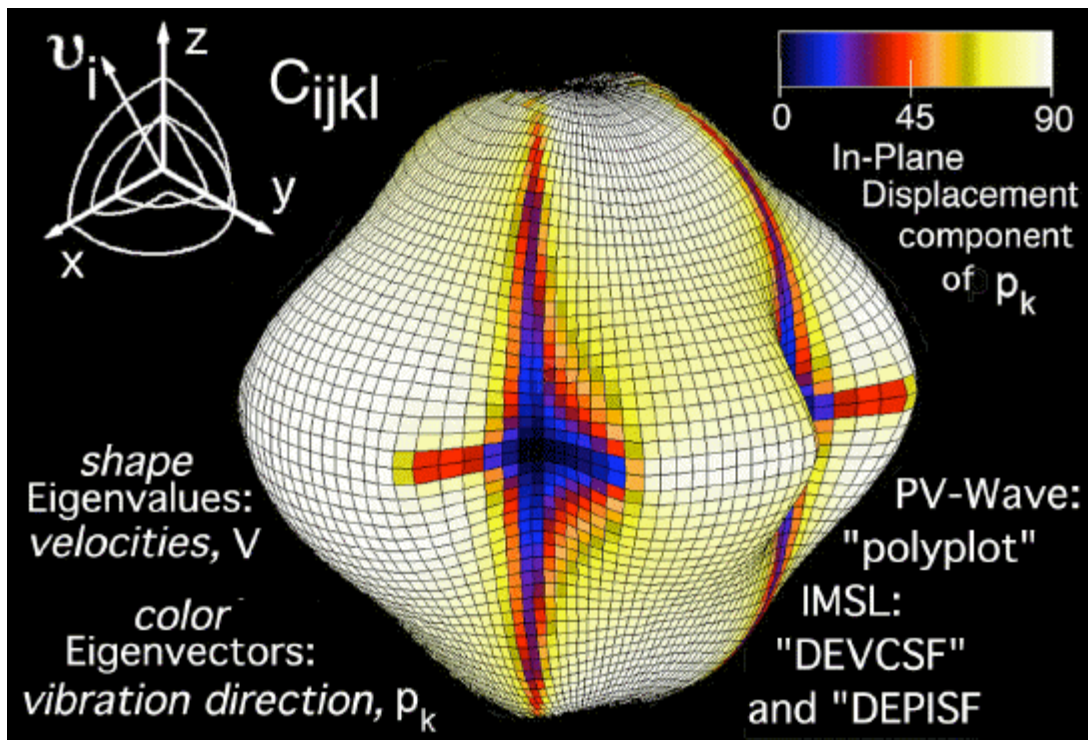


Figure 55. Fourth order stiffness tensor glyph for a single crystal of Calcium Formate (orthorhombic symmetry). Shape of surface maps the wave velocity for the fastest of the two quasi-transverse waves [17,18]. Here only the intermediate wave surface is shown. The outermost and inner most wave surfaces are not shown. Visual Numerics PV-Wave software, Ref. [21], maps the particle vibration directions onto the glyph surface as color: black corresponds to longitudinal (0°) vibration directions and white corresponds to transverse (90°).

Several researchers [17, 18, 19, 20] have used Christoffel's equation to study the symmetries of waves propagating in different crystal class symmetries. A summary of results for different crystal class symmetries is present here as an example.

3D C_{ijkl} Wavesurfaces: Here numerous web links are provided. Wave surface [geometries are defined](#) as it represents the fourth order stiffness tensor, C_{ijkl} . VRML files viewable with Cosmo Plugin ([download for Windows Web browsers](#)) or with the Cortona Plugin ([ParallelGraphics Inc.:](#) for Windows, Mac and MacOS-X). Access details on [how-to-create](#) these wave surfaces. Create your own [C_{ijkl} fourth order tensor glyphs](#) using the Network Programming Interface Builder ([NPIB](#)). Below are archived examples of the most common crystal class symmetries.

- Isotropic (polycrystalline): [Stainless Steel](#)
- Cubic Symmetry: [Aluminum](#)
- Hexagonal Symmetry: [Zinc](#)
- Transversely Isotropic: [Unidirectional Graphite/Epoxy](#) (Fiber Volume Fraction = 66%)
- Tetragonal Symmetry: [Tellurium Dioxide](#): Discussion on wave surface ["cross-overs"](#).
- Orthorhombic Symmetry:
 - Type-1: [Benzene](#) (Most Common: Inner and Intermediate Wave Surfaces Connected)
 - Type-1: [Barium-Yttrium-CopperOxide](#) (Wave Surfaces Connected due to superconducting phase transformation)
 - Type-2: [Calcium Formate](#) (Rarest: All Wave Surfaces Connected Into a Single Surface)
 - Type-3: [Hypothetical](#) (Outer, Intermediate, and Inner Wave Surfaces Not Connected)

- Type-4: [Hypothetical](#) (Outer and Intermediate Wave Surfaces Connected)

The reader interested in the tensor approach to this dynamic problem is encouraged to study references [17, 18, 19]. For the reader only interested in the previous example of the principal stress state, it is not difficult to show that equation (36) reduces to equation (15). This is a simple task using tensor notation. Both equations are rewritten here to facilitate the comparison.

$$[C_{ijkl} v_i v_j - \rho v^2 \delta_{kl}] p_k = 0 \quad (36)$$

$$(\sigma_{ji} - \sigma \delta_{ij}) n_j = 0 \quad (15)$$

This comparison is possible by assigning a double contraction of the direction cosine, "pointing", tensors, \mathbf{V}_i and \mathbf{V}_j , with the fourth order stiffness tensor, C_{ijkl} , where if we let

$$\beta_{kl} = C_{ijkl} v_i v_j, \quad n_k = p_k \quad (37) \text{ and } (38)$$

and the scalar terms

$$\beta = \rho v^2, \quad (39)$$

Eqn. (36) reduces to the same tensor equation that defines the eigen-value problem, Eqn. (15),

$$(\beta_{kl} - \beta \delta_{kl}) n_k = 0 \quad (40).$$

Except for the term, β_{ij} which is contracted with the fourth order stiffness tensor, C_{ijkl} , see Eqn. (37), the β_{ij} term in Eqn. (40) is not just a simple second order tensor like σ_{ij} , but derives its properties from a higher order tensor and hence enjoys a much richer surface topology shown in Fig. 55 than the simple PNS ellipsoid geometry for σ_{ij} .

The fact that Eqn.s (36) and (15) have the same invariant tensoral form supports the idea, proposed in section *Point Stress Tensor Gradients in Three Dimensions*, that a continuous stress gradient in all directions, envisioned as a surface generated by an infinite set of stress quadric surfaces expanding out from the center glyph, would generate a surface similar to an infinite set of 2D plane waves emanating from a point. Indeed the surface generated by Eqn. (36), Fig. 56, starts at a point, which is envisioned as a spherical dilatation constructed of an infinite number of 2D plane waves expanding out in all directions simultaneously. Each of these plane waves travels in a specific direction called the pointing vector, \mathbf{V}_i , at a speed that corresponds to elastic properties in the same direction. Hence, plane waves traveling in different directions in an anisotropic material will travel at different speeds and the continuous collection of all connected plane waves, although initially a sphere, soon deviates into a non-spherical shape simply because a plane wave will travel faster in stiffer directions and slower in less stiff directions. The final result is envisioned as three wave surfaces connected together through their points of degeneracies

as shown in Fig. 56 and also in the schematic in the upper left corner of Fig. 55.

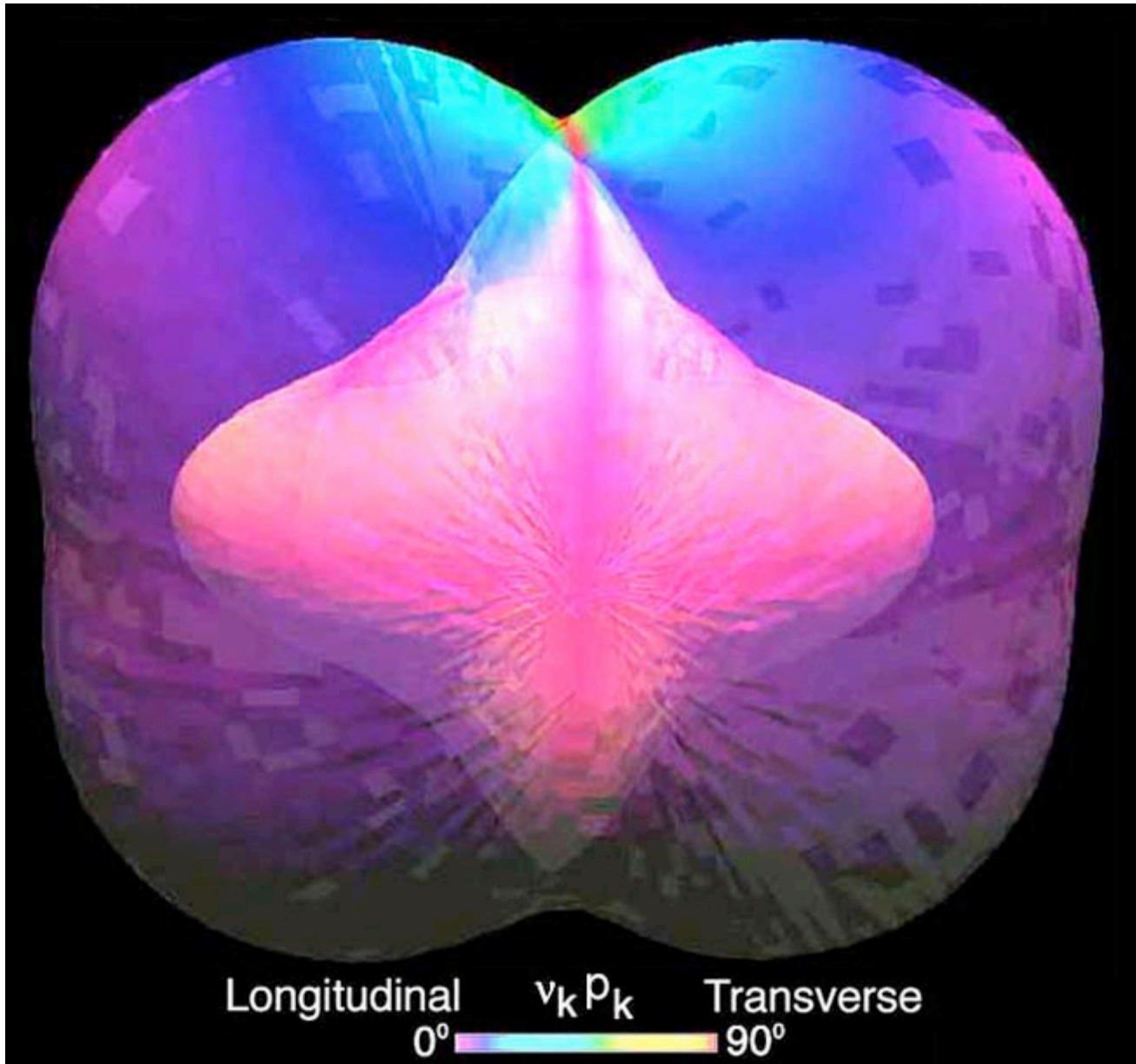


Figure 56. Complete solution to Christoffel's Eqn. (36) for Calcium Formate envisioned using translucency: [VRML-1](#) and [VRML-2](#).

In Fig. 56 the outer two, faster, wave surfaces are shown using translucency so that the inner two, slower, wave surface structures can be seen as a single surface connected to the outer surface. The single connected surface is seen schematically in the upper left corner of Fig. 55 and immersively by using head tracking in a back projected immersive environment. Together these three surfaces are the collection of all eigen-values solutions mapped out in all directions. This is similar to mapping out all solutions to Cauchy's equation, which is equivalent to the statement of equilibrium when mapping out the stress quadric surface, Eqn. (27). Hence the mathematical invariance of Cauchy's equation envisions static equilibrium in Figs 32 and 34, the same as invariance of Christoffel's equation is used to envision dynamic equilibrium in Fig. 56. This supports the idea proposed in the introduction, that "enhanced understanding is realized when graphical models are created together with the development of the

mathematical models". Because Eqn.s (36) and (15) are tensor equations, information embedded in Fig.s 32, 34, and 56 facilitates discovery and insight that transcends presentational value ("pretty pictures").

Envisioning Sixth-Order Stress Induced Anisotropy Tensors, D_{ijklmn}

Following the same idea presented in the development of Eqn. (40), it is possible to show that the C_{ijkl} term in Eqn. (36) is a contraction of a higher order tensor, that is the sixth order tensor, D_{ijklmn} , associated with stress induced anisotropy.

This is on going reserach which will be posted as results become available.

Send comments to: rkriz@vt.edu
Ronald D. Kriz, [Short Bio](#)
Engineering Science and Mechanics
College of Engineering
Virginia Tech
Blacksburg, Virginia 24061
Revised 08/09/06

<http://www.sv.vt.edu/classes/ESM4714/methods/EEG.html>